J Appl Physiol 125: 1944–1967, 2018.
First published September 20, 2018; doi:10.1152/japplphysiol.00095.2018.

RESEARCH ARTICLE | *Vascular Aging*

Computational model-based assessment of baroreflex function from response to Valsalva maneuver

Samuel A. Kosinski,[1] Brian E. Carlson,[1] Scott L. Hummel,[2,3] Robert D. Brook,[2] and Daniel A. Beard[1]

[1]*Molecular and Integrative Physiology, University of Michigan, Ann Arbor, Michigan;* [2]*Internal Medicine and Cardiology, University of Michigan, Ann Arbor, Michigan; and* [3]*Ann Arbor Veterans Affairs Health System, Ann Arbor, Michigan*

Submitted 31 January 2018; accepted in final form 14 September 2018

Kosinski SA, Carlson BE, Hummel SL, Brook RD, Beard DA. Computational model-based assessment of baroreflex function from response to Valsalva maneuver. *J Appl Physiol* 125: 1944–1967, 2018. First published September 20, 2018; doi:10.1152/japplphysiol.00095.2018.—Functional metrics of autonomic control of heart rate, including baroreflex sensitivity, have been shown to be strongly associated with cardiovascular risk. A decrease in baroreflex sensitivity with aging is hypothesized to represent a contributing causal factor in the etiology of primary hypertension. To assess baroreflex function in human subjects, two complementary methods to simulate the response in heart rate elicited by the Valsalva maneuver were developed and applied to data obtained from a cohort of healthy normal volunteers. The first method is based on representing the baroreflex arc as a simple linear filter, transforming changes in arterial pressure to changes in R-R interval. The second method invokes a physiologically based model for arterial mechanics, afferent baroreceptor strain-dependent firing, and control of heart rate via central autonomic response to changes in afferent inputs from aortic and carotid sensors. Analysis based on the linear filter model reveals that the effective response time of the baroreflex arc tends to increase with age in healthy subjects and that the response time/response rate is a predictor of resting systolic pressure. Similar trends were obtained based on the physiologically based model. Analysis of the Valsalva response using the physiologically based model further reveals that different afferent inputs from the carotid sinus and the aortic arch baroreceptors govern different parts of the heart rate response. The observed relationship between baroreflex sensitivity and systolic pressure is surprising because hypertensive subjects were excluded from the study, and there was no observed relationship between arterial pressure and age.

NEW & NOTEWORTHY We introduce two methods to assess baroreflex function from data recorded from human subjects performing the Valsalva maneuver. Results demonstrate that the baroreflex response time tends to increase with age in healthy subjects, that response time represents a predictor of resting systolic pressure, and that the Valsalva response reveals different effects mediated by baroreceptors in the carotid sinus compared with those in the aortic arch.

baroreflex; computational physiology; Valsalva

INTRODUCTION

Stretch receptors in the walls of the aortic arch and the carotid sinus fire in response to changes in arterial wall strain, sending signals that are interpreted by the central nervous system to influence the firing of sympathetic and parasympathetic efferent fibers via the arterial baroreflex system. Increases in arterial pressure, resulting in increased wall strain, result in decreases in heart rate through increased parasympathetic and decreased sympathetic tone. Conversely, a drop in pressure results in an increase in sympathetically and parasympathetically mediated heart rate. The sensitivity of the baroreflex system, measured as the change in heart rate elicited by a given change in arterial pressure, has been shown to be an effective predictor of cardiovascular disease/mortality (16, 17). Predictive relationships between baroreflex sensitivity (BRS) and various metrics of cardiovascular function (ejection fraction, pulmonary wedge pressure, and cardiac work capacity) have been observed (17). BRS has also proven useful in assessing pathophysiological mechanisms underlying orthostatic hypotension (20, 24).

Dysfunction of the baroreflex system has been associated with hypertension in humans. A relationship between increased sympathetic outflow and decreased BRS has been observed in some hypertensive patients (10). An association between BRS and responsiveness to renal denervation therapy in resistant hypertension (36) points to a potential role of the baroreflex system in the etiology of neurogenic hypertension. Indeed, studies by Thrasher (33) demonstrate that surgically induced unloading of arterial baroreceptors causes neurogenic hypertension in animal models. Our theoretical studies support the hypothesis that vascular mechanical remodeling (stiffening of large arteries), resulting in a resetting of baroreflex strain sensitivity, represents a root cause of primary hypertension (2–4, 6, 27).

Baroreflex responsiveness may be assessed by measuring either the direct response of peripheral sympathetic outflow or the heart rate to changes in arterial pressure (29). The present study focuses on the autonomic reflex control of heart rate. A variety of experimental procedures have been applied to perturb pressure and assay a reflex response in heart rate. These approaches include administration of vasodilators and vasoconstrictors such as α-agonists and angiotensin (5, 8, 16, 17). In addition to using pharmacological approaches to alter pressure, early studies required invasive indwelling catheters to measure arterial pressure on a beat-to-beat basis (5, 16, 17). Imholz et al. (14) introduced use of Valsalva maneuver as a noninvasive stimulus and use of finger arterial pressure monitoring for noninvasive pressure measurement. Moreover, just as there exist a variety of approaches to acutely perturb and measure pressure to elicit a response in heart rate, numerous approaches have been applied to analyze the resulting data (7, 18, 26). One approach is to estimate the slope of the change in

Address for reprint requests and other correspondence: D. A. Beard, 2800 Plymouth Rd., Ann Arbor, MI 48105 (e-mail: beardda@umich.edu).

R-R interval versus some measure of arterial pressure. Related definitions of BRS include the slope of the change in R-R interval versus the change in systolic pressure measured over the previous R-R interval (16, 17), the slope of the change in R-R interval versus the systolic pressure measured two beats before a given R-R interval (5), and the slope of R-R interval versus the systolic pressure measured from the previous beat (15). There is some ambiguity in all of these definitions as they are applied to a time window that is not necessarily clearly defined. For example, Kautzner et al. refer to a "period of interest…selected by the operator" (15). There also exist methods of analyzing spontaneous fluctuations that are not subject to influence by choice of protocol or operator bias (23, 26, 35). For example, Westerhof et al. (35) compute the gain as the cross-correlation between R-R interval and systolic pressure at a fixed delay found to show the greatest positive correlation.

The goals of this study are to develop and characterize alternate methods to analyze autonomic reflexes involved in arterial pressure and heart rate dynamics, to apply these methods to data obtained from human subjects undergoing a Valsalva maneuver, and to use computational modeling to improve our understanding of the physiological response to the Valsalva maneuver. We have developed two complementary methods to analyze data on arterial pressure and heart rate that are equivalently and robustly applicable analyzing spontaneous fluctuations as well as larger responses elicited by physiological perturbations (e.g., tilt and Valsalva). Both methods are applied to data obtained using a device for noninvasive measurement of arterial blood pressure (Finometer; Finapres Medical Systems) before, during, and after a Valsalva maneuver in a small cohort of normotensive subjects (14 female, 13 male) ranging in age from 21 to 67 yr. The first method uses a simple linear filter to transform input time course data on arterial pressure to output time courses of heart rate and R-R interval. This method invokes a minimal number of adjustable parameters representing a gain, an offset, and a time constant. The second method uses a mathematical model based on representing physiological mechanisms (4). The physiologically based model invokes additional parameters representing processes associated with arterial mechanics, baroreceptor afferent firing response to arterial strain, and heart rate response to changes in afferent firing. The two methods yield different (related and potentially complementary) metrics of baroreflex sensitivity.

Analysis of data from normotensive subjects reveals *1*) no statistically discernable differences between functional parameters estimated for the female versus male participants; *2*) an increase in baroreflex response time with increasing age; and *3*) a significant relationship between baroreflex function and systolic pressure, with faster responsiveness associated with lower pressure. Furthermore, analysis using the physiologically mechanistic model reveals new insight into features of the Valsalva response, with different inputs from aorta versus carotid sinus dominating different parts of the response. The observed relationship between baroreflex sensitivity and systolic pressure is surprising because hypertensive subjects were excluded from the study, and there was no observed relationship between arterial pressure and age.

METHODS

Data Collection

Healthy subjects (14 female, 13 male) were recruited with exclusion criteria of arterial hypertension, heart disease, history positive for vascular surgery, pulmonary hypertension, aneurism, dissection, stroke, thromboembolism, valvular disease, inherited cardiomyopathy, or connective tissue disease. This investigation was approved by the University of Michigan Institutional Review Board. Written informed consent was obtained from all study participants.

The Valsalva maneuver was utilized to examine blood pressure and heart rate dynamics over a known period of baroreflex activation, while minimizing risk and discomfort for human subjects (19, 30). Subjects performed an ~15-s Valsalva maneuver by bearing down on a closed pipe and mouthpiece fitted with a pressure transducer, to obtain airway pressure. Subjects were asked to maintain a target airway pressure of ~30–40 mmHg. Recorded airway pressure was then employed as an approximate measure of intrathoracic pressure in the analysis described below.

To collect heart rate and arterial pressure data before, during, and after the Valsalva maneuver, a finger cuff arterial pressure monitoring device (Finometer; Finapres Medical Systems) was used to collect a continuous time series of arterial blood pressure and interbeat heart rate through a finger cuff (14, 25). The Finometer directly measures peripheral arterial pressure at the finger cuff while the device provides an estimation of central arterial blood pressure. Measurements were obtained from subjects positioned in a supine manner throughout data collection. Baseline blood pressure and heart rate metrics were collected for 10–15 s, followed by a Valsalva maneuver of consistent airway pressure for another 10–20 s. This duration ensures baroreflex response while minimizing the influences of other reflex responses, such as through chemoreceptors (9). Normal baroreflex thresholds have been outlined as at least 30 mmHg for at least 7 s (21), but these benchmarks may not apply to hypertensive individuals with potential baroreflex dysfunction, as they have not been substantiated in nonnormal subjects. Not all subjects participating in this study were able to reach such thresholds, but that does not necessarily limit the impact of Valsalva on circulatory dynamics.

Time courses of airway pressure, arterial pressure, and heart rate for a typical subject (*subject 4*, female, 42 yr) are shown in Fig. 1. Before the initiation of the Valsalva, heart rate and mean arterial pressures fluctuate around baseline of ~75 mmHg and 60 min^{-1}. The four distinct phases of the physiological response to the Valsalva maneuver are identified (12) as follows.

Phase 1. The rapid increase in thoracic pressure (beginning at time $t = 15.5$ s) causes a transient increase in pressure, due to increased transmural pressure on the great veins, the heart, and the large arteries in the thoracic cavity. In this example, the arterial pressure during the Valsalva period peaks near time $t = 17$ s. This rapid increase in pressure elicits a transient drop in heart rate, which achieves a local minimum at time $t = 18$ s.

Phase 2. After the initial peak in pressure, the effect of increased transmural pressure on restricting flow to the large veins causes a decrease in stroke volume (reflected in a decrease in pulse pressure) and associated drop in mean arterial pressure. Heart rate increases to compensate for this drop in pressure, and by the end of the Valsalva period, heart rate has reached a peak of ~92 min^{-1} in this example. The increase in heart rate that occurs during the Valsalva period can bring about a partial or complete restoration in arterial pressure. [The restoration phase has been distinguished as phase 2b (34).]

Phase 3. When the Valsalva is released (when expiratory pressure drops back to normal baseline), there is a rapid drop in pressure, because preload drops and there is a delay in refilling the large veins that were squeezed during the Valsalva. This drop in pressure may be associated with a second peak in heart rate, occurring at $t = 34$ s in this example.

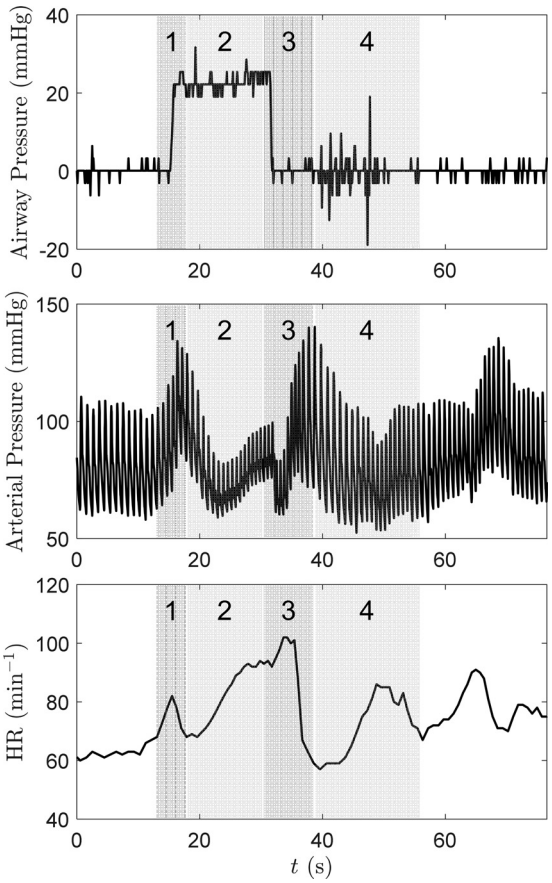

Fig. 1. Arterial pressure and heart rate response to Valsalva maneuver. Measured data are shown for *subject 4* (female, 42 yr old). *Top*: measured expiratory pressure; maintained an ~20-mmHg pressure during the Valsalva period between approximately times $t = 15$ and 31 s. *Middle*: arterial pressure measured by the Finometer device. *Bottom*: measured heart rate (HR) over the observed time course. The four phases described in the text (phases 1–4) of the baroreflex are indicated on the graphs.

Phase 4. When preload is restored, and while heart rate remains elevated, there can be an overshoot in the pressure response, with a local peak in systolic and mean pressure occurring after the release of the Valsalva. This transient increase in pressure is associated with a transient decrease in heart rate, which falls to 57 min^{-1} at $t = 39$ s for this subject. Eventually, the pressures and heart rate restore to their baseline values.

The degree to which individual features described above are pronounced varies from subject to subject. Not all features are detectable in all recordings from all subjects, as discussed below.

Linear Filter Model

We represent the influence of changes in arterial wall strain on heart rate using a simple linear filter governed by the following equation

$$\tau \frac{\mathrm{dRR}(t)}{\mathrm{d}t} = \alpha P_p(t) + R_o - \mathrm{RR}(t) \quad (1)$$

where RR(t) is the R-R interval (heart rate = 1/RR), $P_p(t)$ is the pulse pressure, and α, R_o, and τ are adjustable parameters. Since afferent baroreceptor fibers fire in response to changes in strain, this model assumes that changes in pulse pressure affect changes in heart rate. The parameter α represents the gain, whereas the time constant τ determines how quickly the system responds to changes in pressure. Assuming a piecewise constant right-hand side of *Eq. 1* over an individual beat of duration Δt, *Eq. 1* has the solution

$$\mathrm{RR}(t) = \mathrm{RR}(t-\Delta t)e^{-\Delta t/\tau} + \left(1 - e^{-\Delta t/\tau}\right)\left[\alpha P_p(t-\Delta t) + R_o\right] \quad (2)$$

The linear filter model is fit to measured data by adjusting the parameters α, R_o, and τ for each subject to match the recorded RR(t) to the time series predicted by *Eq. 2*.

Physiologically Based Model

To simulate the physiological processes underlying the baroreflex response, we adapt the baroreflex component of model of Beard et al. (4), which simulates pressure-dependent arterial strain, strain-dependent afferent baroreceptor firing, and the influence of afferent input on the heart rate.

A simple viscoelastic model is used to simulate arterial wall dynamics

$$\mu \frac{\mathrm{d}D}{\mathrm{d}t} = \frac{DP}{2} - kD(D - D_o)^2 \quad (3)$$

where D is the vessel diameter and P is the pressure drop across the wall of the vessel. *Equation 3* assumes a parabolic steady-state pressure-diameter relationship. The parameter μ represents an effective viscosity of the vessel wall, and k and D_o determine the stiffness of the vessel. Figure 2 shows data from Stefanadis et al. (32) used to parameterize the arterial mechanics model of *Eq. 3*. Figure 2*A* shows aortic pressure measured in a control subject, and Fig. 2*B* shows the recorded pressure-diameter loop for the cardiac cycle. Using the measured pressure as an input to the model, the model-predicted pressure-diameter loop is matched to the measured data in Fig. 2*B*, obtained with parameter values $\mu = 2.1$ s·mmHg, $k = 0.505$ mmHg/mm^2, and $D_o = 12.35$ mm. These parameter values are held fixed for the model-based analysis described below. To equivalently represent vessels of different sizes, we introduce a scaled version of *Eq. 3*

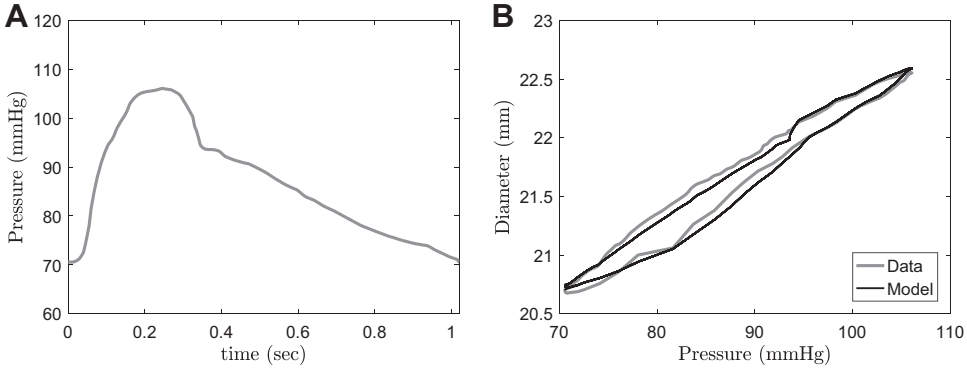

Fig. 2. Arterial diameter-pressure relationship. Arterial pressure and aortic diameter time courses obtained over the cardiac cycle for a normal control subject were obtained from the study of Stefanadis et al. (32; Fig. 7 therein). *A*: arterial pressure wave. *B*: pressure-diameter loop for the cardiac cycle. The model of *Eq. 3* is fit to the data yielding parameter estimates $\mu = 2.1$ s·mmHg, $k = 0.505$ mmHg/mm^2, and $D_o = 12.35$ mm, where the parameter μ represents an effective viscosity of the vessel wall and k and D_o determine the stiffness of the vessel.

$$\mu\dot{d} = \frac{1}{2}dP - k'd\left(d - D'\right)^2$$

where $d = D/D_{\text{ref}}$, $D' = D_d/D_{\text{ref}}$, $k' = kD_{\text{ref}}^2$, and D_{ref} is a reference diameter. For the aorta, using $D_{\text{ref}} = 20$ mm, the scaled mechanics parameters become $k' = 202$ mmHg and $D' = 0.617$. Furthermore, to simulate the different strains experienced by vessels inside the thoracic cavity (including the aortic arch), and those outside (including carotids), we invoke two versions of this vessel model

$$\mu\dot{d}_1 = \frac{1}{2}d_1\left[P_A(t) - P_{\text{th}}(t)\right] - k'd_1\left(d_1 - D'\right)^2$$

$$\mu\dot{d}_2 = \frac{1}{2}d_2P_A(t) - k'd_2\left(d_2 - D'\right)^2 \quad (4)$$

where $P_A(t)$ is the arterial pressure and $P_{\text{th}}(t)$ is the intrathoracic pressure. The nondimensional diameter d_1 represents relative aortic diameter, and d_2 represents the relative (nondimensional) diameter of the carotids. The model assumes that the baroreceptors in each compartment sense the dynamic strain relative to mean strain computed as the running average

$$\frac{d\overline{\varepsilon_1}}{dt} = \left(d_1 - \overline{\varepsilon_1}\right)/\tau_s$$

$$\frac{d\overline{\varepsilon_2}}{dt} = \left(d_2 - \overline{\varepsilon_2}\right)/\tau_s \quad (5)$$

where τ_s is a time constant related to baroreceptor adaptation. The value of this parameter controls how quickly the system adapts to chronic changes in mean pressure, and thus its value does not influence the responses observed over the timescales analyzed here. The instantaneous relative strains are compared with the running averages to compute response functions that are nonzero only when instantaneous strain exceeds the running average

$$\delta_{\varepsilon 1} = \max\left(d_1 - \overline{\varepsilon_1}, 0\right)$$

$$\delta_{\varepsilon 2} = \max\left(d_2 - \overline{\varepsilon_2}, 0\right) \quad (6)$$

The afferent baroreceptor firing rates, f_{BR1} and f_{BR2}, are related to $\delta_{\varepsilon 1}$ and $\delta_{\varepsilon 2}$ by the saturable relationships

$$f_{\text{BR1}} = f_0 s_1 \frac{\delta_{\varepsilon 1}}{\delta_{\varepsilon 1} + \delta_{\varepsilon 0}}$$

$$f_{\text{BR2}} = f_0 s_2 \frac{\delta_{\varepsilon 2}}{\delta_{\varepsilon 2} + \delta_{\varepsilon 0}} \quad (7)$$

where f_0 and $\delta_{\varepsilon 0}$ are parameters defining baroreceptor gain and saturation and s_1 and s_2 represent the fraction of baroreceptor afferents in firing-permissive states. The quantities s_1 and s_2 are governed by

$$\frac{ds_1}{dt} = a\left(1 - s_1\right) - bs_1\frac{\delta_{\varepsilon 1}}{\delta_{\varepsilon 1} + \delta_{\varepsilon 0}}$$

$$\frac{ds_2}{dt} = a\left(1 - s_2\right) - bs_2\frac{\delta_{\varepsilon 2}}{\delta_{\varepsilon 2} + \delta_{\varepsilon 0}} \quad (8)$$

where a and b are rates of baroreceptor activation and deactivation. Parameters τ_s, $\delta_{\varepsilon 0}$, f_0, a, and b were previously estimated on the basis of measurements following step changes in nonpulsatile carotid pressure and ramping pulsatile aortic pressures in vivo (4). The model assumes that sympathetic tone, represented by variable $\phi_{\text{SN}}(t)$, is governed by the following equation

$$\frac{d\phi_{\text{SN}}}{dt} = f_{\text{SN}}\left(1 - \phi_{\text{SN}}\right) - f_1\left[2gf_{\text{BR1}} + 2\left(1 - g\right)f_{\text{BR2}}\right]\phi_{\text{SN}} \quad (9)$$

where f_{SN} and f_1 are model parameters pertaining to autonomic tone and firing rate and g determines the fractional contribution from aortic versus carotid stretch sensors.

The novelty of this model formulation [compared with that given by Beard et al. (4)] is that it invokes two different afferent sensor outputs, associated with the aortic (with firing rate f_{BR1}) and carotid (f_{BR2}) baroreceptors. Here, the simple assumption is made that these two inputs are summed to invoke the combined response. This two-input model is compared with alterative models invoking aortic-only and carotid-only inputs, formulated as follows. The aortic-only model ($g = 1$) accepts input only from the aortic receptors

$$\frac{d\phi_{\text{SN}}}{dt} = f_{\text{SN}}\left(1 - \phi_{\text{SN}}\right) - 2f_1f_{\text{BR1}}\phi_{\text{SN}} \quad (10)$$

and the carotid-only model ($g = 0$) accepts input only from the carotid receptors

$$\frac{d\phi_{\text{SN}}}{dt} = f_{\text{SN}}\left(1 - \phi_{\text{SN}}\right) - 2f_1f_{\text{BR2}}\phi_{\text{SN}} \quad (11)$$

Finally, heart rate (HR) is assumed proportional to the autonomic tone variable

$$\text{HR} = H_0 + H_1\phi_{\text{SN}} \quad (12)$$

where $H_0 = 28$ min^{-1} and $H_1 = 156$ min^{-1} are model parameters. The values of H_0 and H_1 are chosen so that the maximum achievable HR is 184 min^{-1} and HR = 67 min^{-1} at the average resting baseline tone of $\phi_{\text{SN}} = 0.25$.

All parameters invoked in the physiologically based model are listed in Table 1. Here, all parameters except f_{SN}, f_1, and g are identified from previous studies and held fixed for the analysis presented below. Parameters f_{SN}, f_1, and g are adjusted on an individual basis to match the measured HR(t) for a given subject.

This model represents a major simplification of previous models, such as the model of Bugenhagen et al. (6) that accounts for mutually dependent dynamics of parasympathetic and sympathetic efferent firing. While lumping sympathetic and parasympathetic effects into a single autonomic tone variable represents a simplification, the validity of this simplification in the context of this study is demonstrated by its application. The sympathetic and parasympathetic systems are mutually inhibitory and change in opposite directions in response to changes in arterial pressure (6). Thus, the sympathetic tone variable ϕ_{SN} is interpreted as proportional to the cardiac sympathetic firing rate and inversely proportional to the cardiac vagal parasympathetic firing rate.

Table 1. *Physiologically based model parameters*

Name	Explanation	Value	Units
μ	Vessel wall viscosity parameter	2.1	s·mmHg
k'	Vessel wall elasticity parameter	202	mmHg
D'	Vessel wall mechanics parameter	0.6175	Unitless
τ_s	Time constant of afferent adaptation	30*	s
δ_o	Afferent firing sensitivity constant	0.4965	Unitless
a	Afferent fiber activation rate	0.0651	s^{-1}
b	Afferent fiber deactivation rate	0.2004	s^{-1}
f_0	Afferent firing rate factor	300	s^{-1}
H_0	Heart rate parameter	28	min^{-1}
H_1	Heart rate parameter	156	min^{-1}
f_{SN}	Sympathetic tone activation rate	Adjustable	s^{-1}
f_1	Sympathetic tone inhibition rate	Adjustable	Unitless
g	Relative aortic/carotid strength	Adjustable	Unitless

*Results not sensitive to the value of the parameter.

Data Fitting and Parameter Estimation

Both the linear filter model and the physiologically based model are fit to data by adjusting parameters to minimize the sum of squared difference between model output and measured data. For the linear filter model the objective (error) function was calculated as the sum of squared difference between measured and model-predicted RR interval, determined by *Eq. 2*. The parameters τ and α were constrained to be nonnegative using the MATLAB (The MathWorks, Natick, MA) optimization routine fmincon. For the physiologically based model the objective function was calculated as the sum of the squared difference between the measured HR and model-predicted value determined by *Eq. 12*.

RESULTS

Baroreflex Response Assessed by Linear Filter Model

Measured arterial pressure, RR interval, and heart rate for three representative subjects are shown in Fig. 3. Results are shown for the subjects for which the linear filter model of *Eq. 2* shows the lowest (*subject 13*), median (*subject 10*), and highest (*subject 3*) mean square error. The responses of *subjects 13* and *10* show clear increases in heart rate during the Valsalva period and recovery to baseline. The heart rate for *subject 3* follows a less predictable pattern, with relatively little change in heart rate during the measurement. Fits of the linear filter output to data from all 27 subjects are provided in the appendix, Figs. A1–A7.

Summary statistics for the estimated gain α and time constant τ are reported in Table 2. A standard two-sample *t*-test is used to compute *P* values for the probabilities that parameters from male and female groups are drawn from the same statistical distribution. The data reveal no statistically discernable differences in these parameters between the male and female groups. Although the values of τ are lower for the female group than for the male group (2.89 ± 2.47 vs. 5.07 ± 3.57 s, means $\pm$ SD), the difference is not statistically significant ($P = 0.0759$). The difference in the means may be attributed to the fact that the average age of female subjects is ~9 yr less than the average for the male subjects. Trends in the data are explored in more detail in Figs. 4 and 5. Figure 4*A* plots systolic pressure versus age for all study participants, showing no relationship between age and systolic pressure. Nor was there any relationship between age and diastolic or mean pressure (data not shown). Similarly, there was no significant relationship between age and the estimated gain parameter, plotted in Fig. 4*B*. A plot of estimated time constant versus age in Fig. 4*C*, on the other hand, reveals a statistically significant increase in estimated τ with age. Older subjects tend to show a slower response in heart rate to changes in pressure. Similar trends in baroreflex sensitivity (decreasing sensitivity with increasing age) have been observed in previous studies (11, 17).

Data from three outliers, *subjects 6*, *7*, and *17*, are indicated in Fig. 4. *Subject 6* shows an estimated value of τ that is substantially greater than the trend line, with an estimated α that is below the population average. Conversely, *subject 7* shows a relatively rapid response (τ that is substantially lower

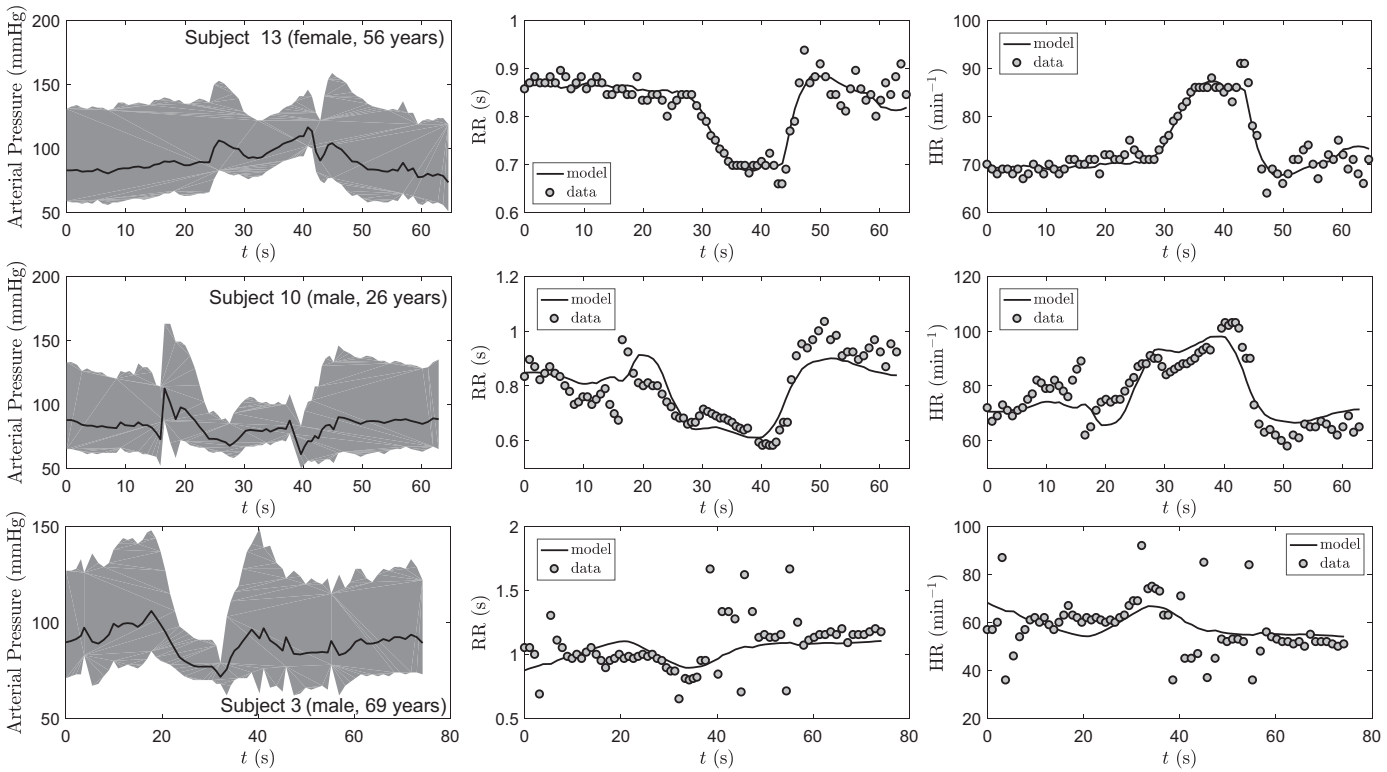

Fig. 3. Arterial pressures, R-R intervals [RR(t)], and heart rate (HR) responses to Valsalva for three representative subjects. *Top*: measured data and linear filter model of *Eqs. 1* and *2* fit for *subject 13*, the subject with the best fit of the model to the RR(t) data. *Middle*: the fit to data from *subject 10* shows the median error value. *Bottom*: the fit to data from *subject 3* shows the highest error (worst fit) for the population. The estimated model parameters for these subjects are as follows: *subject 13*, time constant (τ) = 2.05 s, linear filter offset (R_o) = 0.459 s^{-1}, gain (α) = 5.42 ms/mmHg; *subject 10*, τ = 3.14 s, R_o = 0.405 s^{-1}, α = 6.56 ms/mmHg; and *subject 3*, τ = 10.9 s, R_o = 0.286 s^{-1}, α = 15.7 ms/mmHg.

Table 2. *Summary statistics for baroreflex functional analysis*

	Female	Male	Combined	*P* Value
Demographics				
n	14	13	27	
Age	35.6 ± 16.5	44.5 ± 21.4	39.9 ± 19.2	0.253
Systolic pressure, mmHg	113 ± 10.2	118 ± 14.2	116 ± 12.3	0.278
Diastolic pressure, mmHg	74 ± 8.12	71.7 ± 7.65	73.1 ± 7.87	0.376
Linear filter parameters				
α, ms/mmHg	9.84 ± 4.59	9.84 ± 4.49	9.84 ± 4.45	0.997
τ, s	2.89 ± 2.47	5.07 ± 3.57	3.94 ± 3.19	0.0759
Physiological model parameters				
f_{SN}, s^{-1}	0.041 ± 0.024	0.036 ± 0.030	0.038 ± 0.027	0.656
f_1	0.0046 ± 0.0025	0.0041 ± 0.0027	0.0043 ± 0.0026	0.713
g	0.66 ± 0.16	0.54 ± 0.22	0.59 ± 0.20	0.318

Values are means ± SD; *n* = no. of subjects. Here, α, gain; τ, time constant; f_1, sympathetic tone inhibition rate; f_{SN}, sympathetic tone activation rate; *g*, relative aortic/carotid strength.

than the trend line) and high gain. Examining these outliers, we speculate that there may be an inverse relationship between α and τ. Indeed, a plot of α/τ (Fig. 4*D*) reveals a significant trend of decreasing α/τ with age. In this case the data are fit with a decaying exponential. (The *P* value for the exponential fit is 0.019 compared with $P = 0.069$ for a linear fit.) *Subject 7* is the greatest outlier from the observed trend in α/τ versus age, with the second highest value of α/τ despite being one of the older subjects (age = 59 yr).

Figure 5*A* plots relationships between the baroreflex response time τ and the resting systolic pressure. Here the data reveal a statistically significant relationship between systolic pressure and τ ($P < 0.01$). The strength of this relationship is surprising because a diagnosis of hypertension was an exclusion criterion for the study. The positive correlations between age and τ and between systolic pressure and τ, along with a lack of correlation between age and systolic pressure, indicate that systolic pressure and age are independent predictors of τ. Indeed, combining age and systolic pressure in a multiple regression (Fig. 5*B*) shows that taken together, age and systolic pressure predict τ with a correlation coefficient of 0.627. Furthermore, we notice that the correlation between τ and systolic pressure (Fig. 5*A*) is less strong for the largest values of τ. Excluding the seven individuals with estimated $\tau > 5$ s, the correlation and *P* value for the linear regression become $r = 0.755$ and $P = 1.2 \times 10^{-4}$, respectively.

Prior studies have shown that baroreflex sensitivity diminishes with increasing age and increasing blood pressure (5, 10, 16, 17). However, these studies have reported baroreflex sensitivity in terms of change in heart rate interval per unit change in pressure, measured over a defined time interval. Thus, they do not separate out effects of the speed of response versus overall gain. Our simple linear analysis, which separates the gain and the speed of the response, reveals no significant

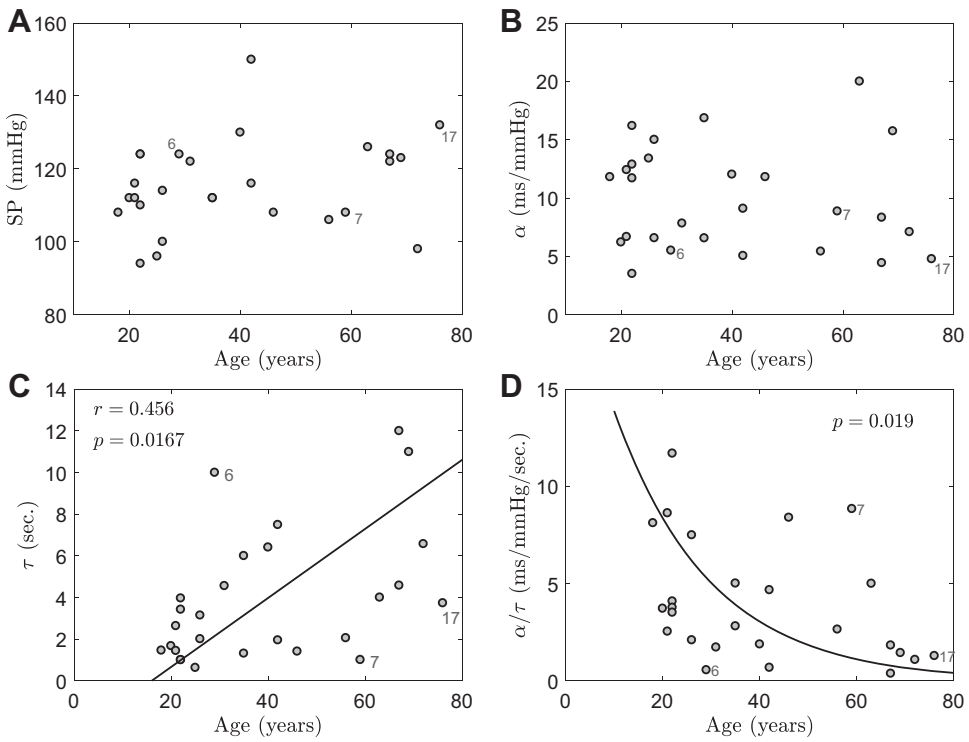

Fig. 4. Relationships among linear filter parameters and subject characteristics. *A*: plot of systolic pressure (SP) vs. age reveals no relationship between these metrics. *B*: plot of estimated filter gain (α) vs. age reveals no relationship between the metrics. *C*: plot of filter time constant (τ) vs. age reveals a statistically significant increase in τ with age, with correlation coefficient and *P* value indicated in plot. *D*: estimated gain divided by time constant (α/τ) is plotted as a function of age, revealing a decreasing trend. These data are fit to a decreasing exponential function $a/\tau \sim \exp(-\text{age}/a)$, with $a = 19.7$ yr. The major outliers (*subjects 6*, *7*, and *17*) from the plots in *C* and *D* are indicated in the figure.

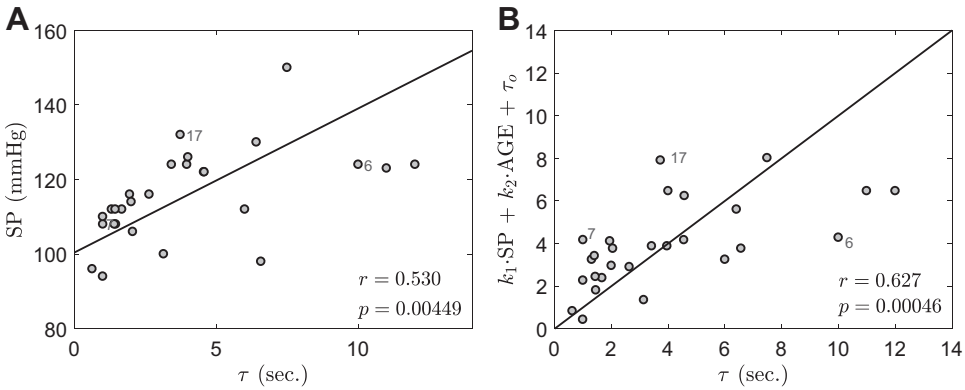

Fig. 5. Predictive relationships associated with filter response time. *A*: systolic pressure (SP) tends to increase in proportion to response time (τ), with $P < 0.01$. *B*: multiple regression for $\tau = k_1 \cdot SP + k_2 \cdot AGE + \tau_0$. Estimated regression coefficients are $k_1 = 0.115$ s/mmHg, $k_2 = 0.0575$ s/yr, and $\tau_0 = -11.6$ s. The major outliers from the plots in Fig. 4 are indicated.

relationships between the filter gain α and age or between α and blood pressure. These findings indicate that the response time, rather than the gain, is the more important indicator of changes in baroreflex function that occur with age and changes in cardiovascular health.

Baroreflex Response Assessed by Physiologically Based Model

The physiologically based model uses the measured expiratory pressure (P_{th}) as a model input via *Eq. 4*, in addition to the measured arterial pressure, to predict heart rate (HR). As an illustrative example, arterial pressure, predicted aortic and carotid diameters, and heart rate are shown in Fig. 6 for *subject 4*. The measured expiratory pressure for this subject is shown in Fig. 1. The simulated diameters (Fig. 6*B*) show that during the Valsalva period, the influence of the compressive pressure results in lower relative diameters for the aorta compared with the carotids. When the Valsalva is released, the carotid strain is predicted to drop sharply as the arterial pressure drops sharply. However, while the carotid strain is dropping (around t = 32 s), the aortic strain is predicted to be increasing because of the release of the compressive pressure associated with the Valsalva.

The consequences of different strain signals originating from the aortic versus carotid strain sensors are explored in Fig. 6*C*. The predicted heart rate associated with the aortic-only model ($g = 1$) does not capture the peak in heart rate that follows the release of the Valsalva, because the aortic strain does not experience the rapid drop predicted for the carotid. Although the carotid-only model ($g = 0$) is able to capture the post-Valsalva heart rate peak, the carotid-only model predicts an initial drop in heart rate that is too large and too late in the early phase 2 response. Only the combined model (Fig. 6*D*, $g = 0.5$) is able to effectively capture all features of the observed heart rate response.

The physiologically based model was applied to the same data set analyzed using the linear filter model, by adjusting the three parameters f_{SN}, f_1, and g on an individual basis to match

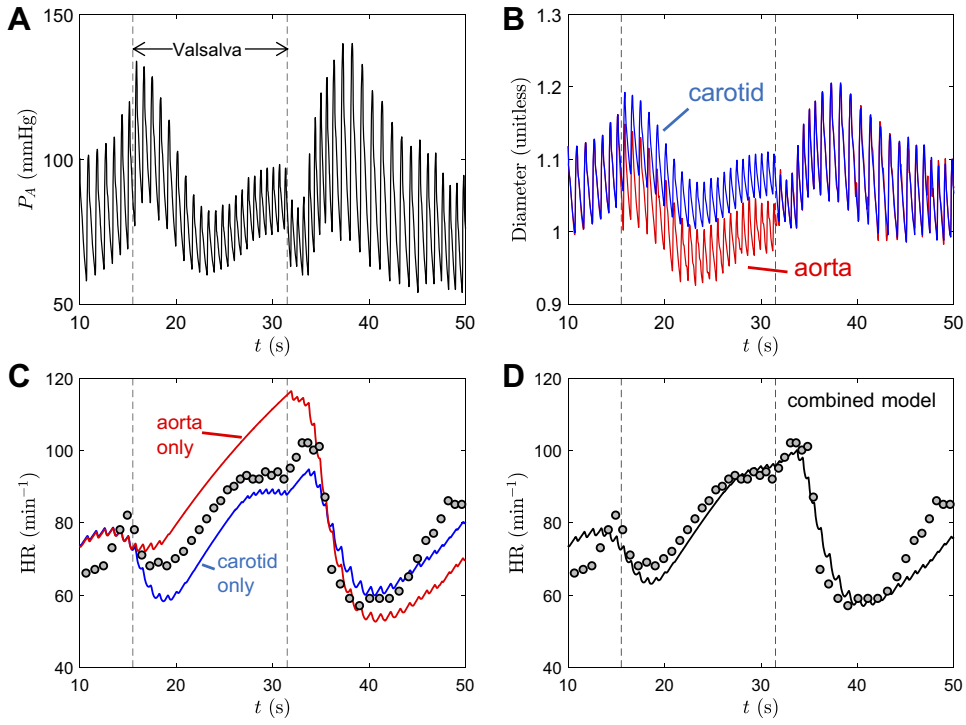

Fig. 6. Analysis of baroreflex response using physiologically based model. *A*: arterial pressure (P_A) measured by Finometer for *subject 4*. *B*: diameters for the aorta and carotids are predicted from *Eq. 4*. The relative (unitless) diameters are identical for the period preceding the Valsalva. During the Valsalva, the relative aortic diameter is lower than that of the carotids because of the external pressure acting to compress the vessels in the thoracic cavity. *C*: the heart rate (HR) response predicted by the physiologically based model is compared with the measure data for the aortic-only and carotid-only versions of the model. *D*: the heart rate response predicted by the physiologically based model is compared with the measured data for the combined (aortic + carotid) version of the model. Values for adjustable model parameters are as follows: sympathetic tone activation rate (f_{SN}) = 0.0365 s^{-1}, sympathetic tone inhibition rate (f_1) = 0.0052, and relative aortic/carotid strength (g) = 0.35. The window over which the Valsalva maneuver is executed is indicated by dashed lines in all panels.

the measured HR(t) for each subject. Model fits for all 27 subjects are shown in Figs. A8–A14 of the appendix. Statistics for model parameters are summarized in Table 2. As for the simple filter model, we find no significant differences between male and female groups (2-sample t-test).

Figure 7 illustrates a variety of trends observed in the parameter estimates for the physiologically based model. Figure 7*A* shows that there is a strong correlation between the rates f_{SN} and f_1. This is not surprising since these parameters, invoked in *Eq. 9*, represent opposing influences on autonomic tone. For the system to attain a resting heart rate in a physiologically reasonable range, these rates increase and decrease in approximate proportion. Since these parameters govern the autonomic response rate, we expected to see a relationship between their values and age, similar to the relationship between age and the time constant τ from the linear filter model. Indeed, as illustrated in Fig. 7, *B* and *C*, the estimated rates f_{SN} and f_1 tend to decrease with age. Figure 7*D* shows that $1/f_{SN}$ from the physiologically based model is strongly correlated with τ estimated from the linear filter model. This correlation is expected because both τ and $1/f_{SN}$ represent rate constants governing the rate of response of the respective models to changes in pressure.

Although the plots in Fig. 7 reveal significant trends in the rates f_{SN} and f_1 that govern how the central nervous system processes and responds to afferent inputs, these relationships should not be interpreted as necessarily reflecting changes to central autonomic function occurring with age. Since independent data on the mechanical properties of the large arteries in the individual subjects were not available, the model fits using the physiologically based model employed fixed parameters (μ, k', and D', Table 1) to represent mechanical properties of the aorta and carotid sinus. Furthermore, since independent data on afferent firing were not obtained, parameters governing how afferent firing responds to changes in strain (τ_s, δ_o, a, b, and f_o) were held fixed. Thus, this model analysis is not able to detect any potential differences in afferent function that may underlie the individual variability in the baroreflex response observed in this study. The differences and trends in estimated values of f_{SN}, f_1, and g may more accurately reflect differences in the arterial mechanical properties or afferent strain sensor properties. For example, a relatively slow response time, reflected in a large value of τ for the linear filter model, and slow rate constants (f_{SN} and f_1) for the physiologically based model, may mechanistically arise from relatively high values of effective stiffness and/or viscosity of the walls of the large arteries associated with the strain sensors. In other words, in the present analysis, variabilities in the central physiologically based model parameters f_{SN} and f_1, or equivalently the filter model time constant τ, are used as proxies to represent potential variability at any stage of the baroreflex arc: from arterial wall mechanics, to afferent firing dynamics, to central autonomic function. Differences in estimated values of these parameters reflect differences in overall responsiveness of the baroreflex system to changes in arterial pressure but do not necessarily pinpoint the underlying sources of variability.

DISCUSSION

We have introduced two methods to assess baroreflex function from data on arterial pressures, heart rate, and expiratory pressure occurring with the Valsalva maneuver in human subjects. The two methods, one based on a phenomenological linear filter model of the baroreflex arc and one based on a physiologically based model, provide similar insights into relationships between the responsiveness of the baroreflex system and age and the responsiveness of the system and systolic arterial pressures.

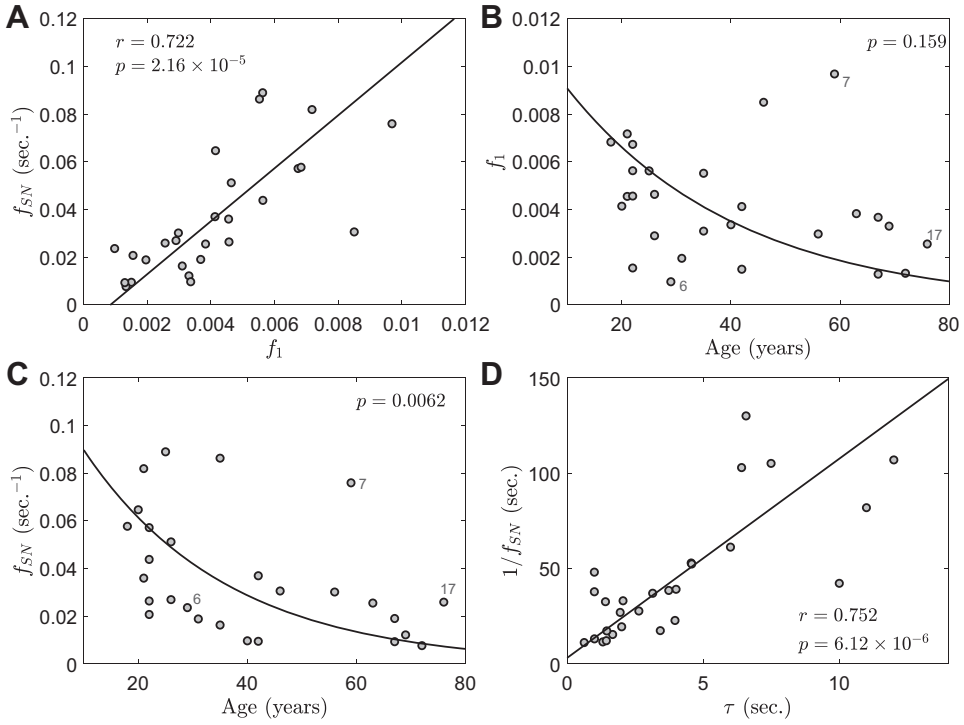

Fig. 7. Relationships among linear filter parameters, physiologically based model parameters, and subject characteristics. *A*: plot of estimated sympathetic tone activation rate (f_{SN}) vs. sympathetic tone inhibition rate (f_1) for the physiologically based model (representing rates of increase and decrease in sympathetic tone) reveals a high degree of correlation. *B*: estimated f_1 as a function of age is matched to a decaying exponential $f_1 \sim \exp(-\text{age}/a)$, with $a = 31.5$ yr. *C*: estimated f_{SN} as a function of age is matched to a decaying exponential $f_{SN} \sim \exp(-\text{age}/a)$, with $a = 26.4$ yr. The exponential decrease is shown to be statistically significant for f_{SN} ($P < 0.01$), but not for f_1. These trends are closely related to the observed correlation between the filter response time (τ) and age illustrated in Fig. 4. *D*: estimated τ (from the linear filter analysis) is closely correlated with $1/f_{SN}$, estimated using the physiologically based model.

Linear Filter Model

The simple linear filter model for the heart rate response to changes in pressure of *Eq. 1* distinguishes parameters representing response time (τ) from gain (α). Previous analyses conflate these components into a baroreflex sensitivity parameter. Our analysis predicts that the response rate (captured by τ) reflects changes to the baroreflex arc that occur with aging, whereas the gain parameter (α) shows no clear trend with age. Difference in response time may be related to differences in viscoelastic properties of vessels containing the stretch receptors or may be related to difference in central autonomic function.

Findings illustrated in Fig. 5 indicating that τ is associated with resting systolic pressure in normal subjects point to the potential utility of this parameter as a predictor of cardiovascular risk. Future larger-scale studies are needed to determine how baroreflex response time [and other metrics derived from this analysis such as gain (α)] may or may not be useful in assessing cardiovascular fitness and risk. Based on the relationship observed in Fig. 5*A*, we speculate that this analysis may be able to reveal the degree to which baroreflex dysfunction contributes to development of hypertension.

Physiologically Based Model

Although the physiologically based model is designed to capture baroreflex function with more mechanistic meaning than the simple linear filter model, it should not be interpreted as providing a quantitatively better match to the data than the simpler model. The physiologically based model does not tend to fit the Valsalva data any better (or worse) than the simpler model. Yet it does potentially reveal more insight into physiological function than the linear filter. For example, the physiologically based model analysis was used to illustrate that different signals from carotid versus aorta are important in governing the response to Valsalva. Previous studies have speculated that carotid versus aortic afferents respond in opposite ways during the initial phase of the Valsalva response (31). Our analysis provides a quantitative estimation of how arterial strain in the carotid sinus and aortic arch tends to change in opposite directions not only in the initial phase of the Valsalva but also when the Valsalva is released. In the initial phase, the increase in arterial pressure causes an overall distension in carotid diameters that is not seen in the aortic arch due to external compression from the elevated thoracic pressure. When the Valsalva is released, the drop in thoracic pressure allows the aortic diameter averaged over the cardiac cycle to increase, even as the mean arterial pressure temporarily drops. For the first few seconds following release of the Valsalva only the carotid baroreceptors are able to sense a decrease in average pressure/strain, and thus the carotid baroreceptors are responsible for the transient increase in heart rate that occurs following the release of the Valsalva.

The major limitation of the physiologically based model analysis is that the model invokes a number of parameters that cannot be estimated from the data obtained in this study. Specifically, parameters representing arterial mechanical properties (μ, k', and D') are set to values obtained from analysis of a healthy individual. Parameters associated with the afferent response to strain rate (τ_s, δ_o, a, b, and f_0) are set to values obtained from studies on large animals (4). By adjusting parameters (f_{SN}, f_1, and g) that govern the response of autonomic tone to fit data from individuals, our analysis is not able to capture any variability in responses that may be governed by differences in mechanical properties and/or afferent strain sensor function. In other words, our analysis lumps likely sources of variability into the parameters representing effector response. Given the large number of parameters (fixed and adjusted), there are likely to be multiple combinations of parameters that could be assigned as adjustable to fit the data. Evaluating which combinations could be used and which could not would be a computationally expensive process that is beyond the scope of the present study. For example, although differences in arterial mechanical properties may underlie differences in baroreflex responses (13, 22, 28), the present analysis is not able to detect this or other potential mechanisms underlying the variability in the population.

Similarly, the linear filter model lumps a series of physiological functions (arterial strain, afferent firing, central processing, and efferent output) into a phenomenological response captured by a simple linear filter. The linear filter model has the advantage that its relatively few parameters may be identified from the time course data obtained here. On the other hand, the greater mechanistic fidelity of the physiologically based model provides a scaffold on which different sources of variability can be accounted for, given independent data on the subsystems from which the physiological model is constructed. For example, independent measurements of arterial stiffness (1) could be incorporated into the individual parameterization of the physiologically based model to more effectively capture the physiological basis for individual variability in the baroreflex response.

Although the model is able to at least qualitatively represent the observed response for most subjects, for several of the cases the model fails to capture the observed trends. Many subjects show a characteristic oscillation in heart rate during the pre-Valsalva period (cf. *subjects 2*, *8*, *12*, and *19*). These oscillations are likely associated with respiration, a phenomenon not accounted for in the model. Furthermore, many subjects show a transient peak in heart rate immediately preceding the Valsalva (cf. Fig. 6). This spike in heart rate is associated with a rapid inhalation taken in preparation for the Valsalva. Again, this phenomenon is not accounted for in our model. Moreover, analysis for several subjects reveals an inability to effectively capture the heart rate response during and after the Valsalva period. For example, the physiologically based model largely fails to represent the heart rate dynamics of *subject 1*, for which the arterial pressure did not show the expected characteristic pattern illustrated in Fig. 6. Specifically, for this subject, mean pressure increases immediately at the onset of the Valsalva maneuver as it does for most subjects. However, although the heart rate gradually increases during the Valsalva period, neither the pulse pressure nor the mean pressure drop substantially, resulting in an inability of the model to capture the response. Although the linear filter model for this subject does a better job of matching the data, it still fails to match the full extent of increase in heart rate that occurred during the Valsalva.

Subjects 7 and *25* are additional examples for whom neither the linear filter nor the physiologically based model effectively captures the data. Similar to the pressure recorded for *subject 1*, the pressures do not drop substantially during the Valsalva

period for either of these subjects. (Compare the pressures in Fig. A14 for *subjects 25* and *26*.) The fit to the data for *subject 7* using the physiological model (Fig. A9) yields values of f_{SN} and f_1 that are outliers in the plots in Fig. 4 and result in rapid oscillations in the model-predicted HR(t).

Limitations of Study

In addition to the simplifying assumptions invoked in the model analyses discussed in METHODS, the conclusions of this study are influenced and limited by the relatively small cohort of subjects and exclusion criteria used to define that cohort. The finding that age and systolic blood pressure are uncorrelated, for example, should not be taken as reflecting the broader population because hypertensive subjects were excluded from the study. Furthermore, given the small size of the study, it is not possible to control for other hidden correlates of arterial pressure and autonomic function, such as exercise training, race, body mass index, etc. Since this study was (by design) biased against potentially observing a relationship between age and arterial pressure, it is unknown how the observed trends in autonomic function vary in the broader population. We hypothesize that suppressed autonomic control of heart rate is a contributing factor to the etiology of primary hypertension, rather than only a compensatory sequela. That we observe relationships between reduced autonomic responsiveness and age and between reduced autonomic responsiveness and systolic pressure is consistent with the specific hypothesis that suppression of autonomic reflexes occurs independently of and can precede hypertension. Further testing of these hypotheses will require substantially larger-scale studies.

Major Findings

The major findings of the study can be summarized as follows.

1) The effective response time of the baroreflex arc tends to increase with age in healthy subjects (Fig. 4*C*). Equivalently, the effective response rate decreases with age.
2) The response time/response rate is a predictor of systolic pressure (Fig. 5*A*) based on observations from a group of 27 healthy volunteers.
3) Analysis of the Valsalva response using a physiologically based model (Fig. 6) reveals that different afferent inputs from the carotid sinus and the aortic arch baroreceptors govern different parts of the heart rate response.

APPENDIX

This appendix contains Figs. A1–A14, plotting the fits of the linear filter model and the physiologically based model to the data from the 27 subjects analyzed in this study. Data collected from all subjects are freely available on PhysioNet.org (9a; https://physionet.org/physiobank/database/rvmh1/).

GRANTS

This work was supported by NIH National Heart, Lung, and Blood Institute Grant HL-139813 to D.A. Beard.

DISCLOSURES

No conflicts of interest, financial or otherwise, are declared by the authors.

AUTHOR CONTRIBUTIONS

S.A.K., B.E.C., S.L.H., R.D.B., and D.A.B. conceived and designed research; S.A.K. performed experiments; S.A.K. and D.A.B. analyzed data; S.A.K. and D.A.B. interpreted results of experiments; S.A.K. and D.A.B. prepared figures; S.A.K. and D.A.B. drafted manuscript; S.A.K., B.E.C., S.L.H., R.D.B., and D.A.B. edited and revised manuscript; S.A.K., B.E.C., S.L.H., R.D.B., and D.A.B. approved final version of manuscript.

ENDNOTE

At the request of the authors, readers are herein alerted to the fact that additional materials related to this manuscript may be found at PhysioNet.org, which at the time of publication they indicate is: https://physionet.org/physiobank/database/rvmh1/. These materials are not a part of this manuscript and have not undergone peer review by the American Physiological Society (APS). APS and the journal editors take no responsibility for these materials, for the Web site address, or for any links to or from it.

REFERENCES

1. **Aquaro GD, Cagnolo A, Tiwari KK, Todiere G, Bevilacqua S, Di Bella G, Ait-Ali L, Festa P, Glauber M, Lombardi M.** Age-dependent changes in elastic properties of thoracic aorta evaluated by magnetic resonance in normal subjects. *Interact Cardiovasc Thorac Surg* 17: 674–679, 2013. doi:10.1093/icvts/ivt261.
2. **Beard DA.** Tautology vs. physiology in the etiology of hypertension. *Physiology (Bethesda)* 28: 270–271, 2013. doi:10.1152/physiol.00038.2013.
3. **Beard DA, Mescam M.** Mechanisms of pressure-diuresis and pressure-natriuresis in Dahl salt-resistant and Dahl salt-sensitive rats. *BMC Physiol* 12: 6, 2012. doi:10.1186/1472-6793-12-6.
4. **Beard DA, Pettersen KH, Carlson BE, Omholt SW, Bugenhagen SM.** A computational analysis of the long-term regulation of arterial pressure. *F1000 Res* 2: 208, 2013. doi:10.12688/f1000research.2-208.v1.
5. **Bristow JD, Honour AJ, Pickering GW, Sleight P, Smyth HS.** Diminished baroreflex sensitivity in high blood pressure. *Circulation* 39: 48–54, 1969. doi:10.1161/01.CIR.39.1.48.
6. **Bugenhagen SM, Cowley AW Jr, Beard DA.** Identifying physiological origins of baroreflex dysfunction in salt-sensitive hypertension in the Dahl SS rat. *Physiol Genomics* 42: 23–41, 2010. doi:10.1152/physiolgenomics.00027.2010.
7. **Castiglioni P, Di Rienzo M, Parati G.** How should the baroreflex sensitivity on the heart be estimated? *J Electrocardiol* 44: 391–392, 2011. doi:10.1016/j.jelectrocard.2011.01.006.
8. **Ebert TJ, Cowley AW Jr.** Baroreflex modulation of sympathetic outflow during physiological increases of vasopressin in humans. *Am J Physiol Heart Circ Physiol* 262: H1372–H1378, 1992. doi:10.1152/ajpheart.1992.262.5.H1372.
9. **Eckberg DL, Sleight P.** *Human Baroreflexes in Health and Disease*. Oxford, UK: Clarendon, 1992.

9a. **Goldberger AL, Amaral LA, Glass L, Hausdorff JM, Ivanov PC, Mark RG, Mietus JE, Moody GB, Peng CK, Stanley HE.** PhysioBank, PhysioToolkit, and PhysioNet: components of a new research resource for complex physiologic signals. *Circulation* 101: e215–e220, 2000. doi:10.1161/01.CIR.101.23.e215.

10. **Goldstein DS.** Arterial baroreflex sensitivity, plasma catecholamines, and pressor responsiveness in essential hypertension. *Circulation* 68: 234–240, 1983. doi:10.1161/01.CIR.68.2.234.
11. **Gribbin B, Pickering TG, Sleight P, Peto R.** Effect of age and high blood pressure on baroreflex sensitivity in man. *Circ Res* 29: 424–431, 1971. doi:10.1161/01.RES.29.4.424.
12. **Hamilton WF, Woodbury RA, Harper HT Jr.** Physiologic relationships between intrathoracic, intraspinal and arterial pressures. *JAMA* 107: 853–856, 1936. doi:10.1001/jama.1936.02770370017005.
13. **Hunt BE, Farquhar WB, Taylor JA.** Does reduced vascular stiffening fully explain preserved cardiovagal baroreflex function in older, physically active men? *Circulation* 103: 2424–2427, 2001. doi:10.1161/01.CIR.103.20.2424.
14. **Imholz BP, van Montfrans GA, Settels JJ, van der Hoeven GM, Karemaker JM, Wieling W.** Continuous non-invasive blood pressure monitoring: reliability of Finapres device during the Valsalva manoeuvre. *Cardiovasc Res* 22: 390–397, 1988. doi:10.1093/cvr/22.6.390.
15. **Kautzner J, Hartikainen JE, Camm AJ, Malik M.** Arterial baroreflex sensitivity assessed from phase IV of the Valsalva maneuver. *Am J Cardiol* 78: 575–579, 1996. doi:10.1016/S0002-9149(96)00370-0.
16. **La Rovere MT, Bigger JT Jr, Marcus FI, Mortara A, Schwartz PJ; ATRAMI (Autonomic Tone and Reflexes After Myocardial Infarction) Investigators.** Baroreflex sensitivity and heart-rate variability in

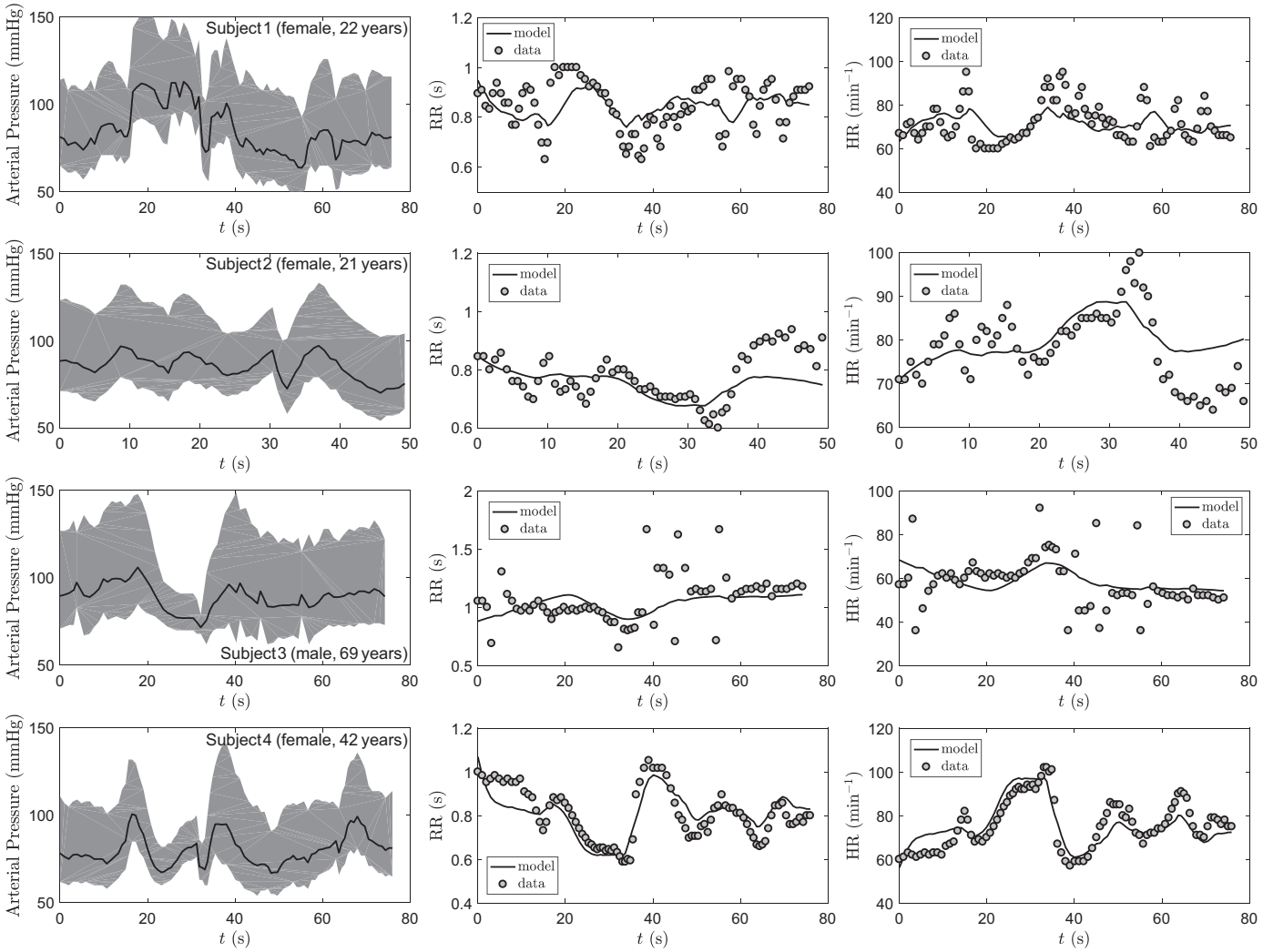

Fig. A1. Arterial pressures, R-R intervals, heart rate responses to Valsalva, and linear filter model fits for *subjects 1–4*. Panels at *left* illustrate measured arterial pressure, panels in *middle* illustrate measured R-R interval (RR) and fits of *Eq. 2*, and panels at *right* show the measured and model-fit heart rate (HR).

prediction of total cardiac mortality after myocardial infarction. *Lancet* 351: 478–484, 1998. doi:10.1016/S0140-6736(97)11144-8.

17. **La Rovere MT, Specchia G, Mortara A, Schwartz PJ.** Baroreflex sensitivity, clinical correlates, and cardiovascular mortality among patients with a first myocardial infarction. A prospective study. *Circulation* 78: 816–824, 1988. doi:10.1161/01.CIR.78.4.816.
18. **Laude D, Elghozi JL, Girard A, Bellard E, Bouhaddi M, Castiglioni P, Cerutti C, Cividjian A, Di Rienzo M, Fortrat JO, Janssen B, Karemaker JM, Lefthériotis G, Parati G, Persson PB, Porta A, Quintin L, Regnard J, Rüdiger H, Stauss HM.** Comparison of various techniques used to estimate spontaneous baroreflex sensitivity (the EuroBaVar study). *Am J Physiol Regul Integr Comp Physiol* 286: R226–R231, 2004. doi:10.1152/ajpregu.00709.2002.
19. **Levin AB.** A simple test of cardiac function based upon the heart rate changes induced by the Valsalva maneuver. *Am J Cardiol* 18: 90–99, 1966. doi:10.1016/0002-9149(66)90200-1.
20. **Mattace-Raso FU, van den Meiracker AH, Bos WJ, van der Cammen TJ, Westerhof BE, Elias-Smale S, Reneman RS, Hoeks AP, Hofman A, Witteman JC.** Arterial stiffness, cardiovagal baroreflex sensitivity and postural blood pressure changes in older adults: the Rotterdam study. *J Hypertens* 25: 1421–1426, 2007. doi:10.1097/HJH.0b013e32811d6a07.
21. **McIntosh HD, Burnum JF, Hickam JB, Warren JV.** Circulatory changes produced by the Valsalva maneuver in normal subjects, patients with mitral stenosis, and autonomic nervous system alterations. *Circulation* 9: 511–520, 1954. doi:10.1161/01.CIR.9.4.511.
22. **Monahan KD, Dinenno FA, Seals DR, Clevenger CM, Desouza CA, Tanaka H.** Age-associated changes in cardiovagal baroreflex sensitivity are related to central arterial compliance. *Am J Physiol Heart Circ Physiol* 281: H284–H289, 2001. doi:10.1152/ajpheart.2001.281.1.H284.
23. **Müller A, Morley-Davies A, Barthel P, Hnatkova K, Bauer A, Ulm K, Malik M, Schmidt G.** Bivariate phase-rectified signal averaging for assessment of spontaneous baroreflex sensitivity: normalization of the results. *J Electrocardiol* 45: 77–81, 2012. doi:10.1016/j.jelectrocard.2011.07.010.
24. **Olufsen MS, Tran HT, Ottesen JT, Lipsitz LA, Novak V; Research Experiences for Undergraduates Program.** Modeling baroreflex regulation of heart rate during orthostatic stress. *Am J Physiol Regul Integr Comp Physiol* 291: R1355–R1368, 2006. doi:10.1152/ajpregu.00205.2006.
25. **Parati G, Casadei R, Groppelli A, Di Rienzo M, Mancia G.** Comparison of finger and intra-arterial blood pressure monitoring at rest and during laboratory testing. *Hypertension* 13: 647–655, 1989. doi:10.1161/01.HYP.13.6.647.
26. **Parati G, Di Rienzo M.** Assessing spontaneous baroreflex function: methodological considerations. *Clin Sci (Lond)* 103: 89–91, 2002. doi:10.1042/cs1030089.
27. **Pettersen KH, Bugenhagen SM, Nauman J, Beard DA, Omholt SW.** Arterial stiffening provides sufficient explanation for primary hypertension. *PLOS Comput Biol* 10: e1003634, 2014. doi:10.1371/journal.pcbi.1003634.
28. **Pierce GL, Harris SA, Seals DR, Casey DP, Barlow PB, Stauss HM.** Estimated aortic stiffness is independently associated with cardiac baroreflex sensitivity in humans: role of ageing and habitual endurance exercise. *J Hum Hypertens* 30: 513–520, 2016. doi:10.1038/jhh.2016.3.

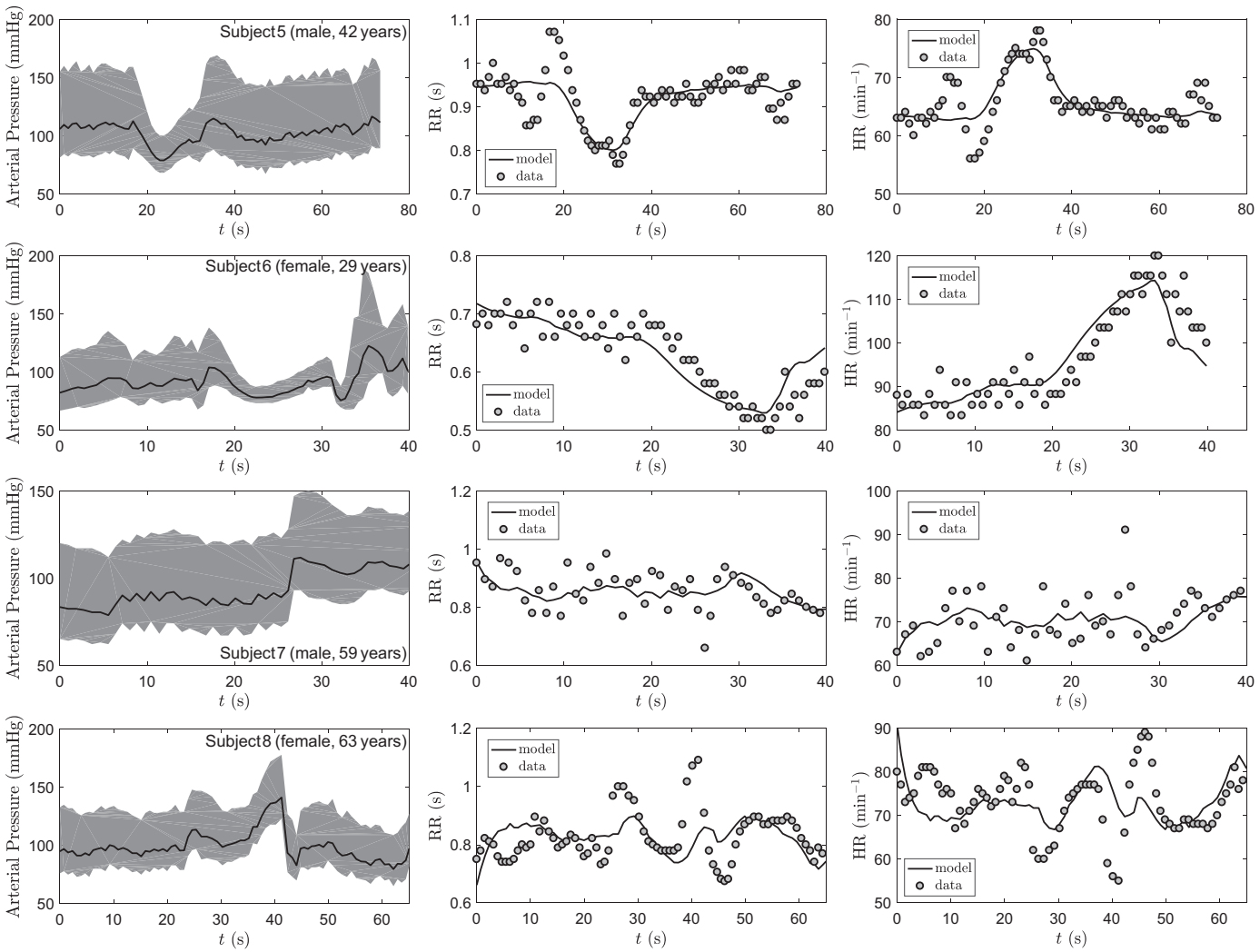

Fig. A2. Arterial pressures, R-R intervals, heart rate responses to Valsalva, and linear filter model fits for *subjects 5–8*. Panels at *left* illustrate measured arterial pressure, panels in *middle* illustrate measured R-R interval (RR) and fits of *Eq. 2*, and panels at *right* show the measured and model-fit heart rate (HR).

29. **Rudas L, Crossman AA, Morillo CA, Halliwill JR, Tahvanainen KU, Kuusela TA, Eckberg DL.** Human sympathetic and vagal baroreflex responses to sequential nitroprusside and phenylephrine. *Am J Physiol Heart Circ Physiol* 276: H1691–H1698, 1999. doi:10.1152/ajpheart.1999.276.5.H1691.
30. **Sharpey-Schafer EP.** Effects of Valsalva's manoeuvre on the normal and failing circulation. *BMJ* 1: 693–695, 1955. doi:10.1136/bmj.1.4915.693.
31. **Smith ML, Beightol LA, Fritsch-Yelle JM, Ellenbogen KA, Porter TR, Eckberg DL.** Valsalva's maneuver revisited: a quantitative method yielding insights into human autonomic control. *Am J Physiol Heart Circ Physiol* 271: H1240–H1249, 1996. doi:10.1152/ajpheart.1996.271.3.H1240.
32. **Stefanadis C, Stratos C, Vlachopoulos C, Marakas S, Boudoulas H, Kallikazaros I, Tsiamis E, Toutouzas K, Sioros L, Toutouzas P.** Pressure-diameter relation of the human aorta. A new method of determination by the application of a special ultrasonic dimension catheter. *Circulation* 92: 2210–2219, 1995. doi:10.1161/01.CIR.92.8.2210.
33. **Thrasher TN.** Unloading arterial baroreceptors causes neurogenic hypertension. *Am J Physiol Regul Integr Comp Physiol* 282: R1044–R1053, 2002. doi:10.1152/ajpregu.00431.2001.
34. **Tiecks FP, Lam AM, Matta BF, Strebel S, Douville C, Newell DW.** Effects of the Valsalva maneuver on cerebral circulation in healthy adults. A transcranial Doppler study. *Stroke* 26: 1386–1392, 1995. doi:10.1161/01.STR.26.8.1386.
35. **Westerhof BE, Gisolf J, Stok WJ, Wesseling KH, Karemaker JM.** Time-domain cross-correlation baroreflex sensitivity: performance on the EUROBAVAR data set. *J Hypertens* 22: 1371–1380, 2004. doi:10.1097/01.hjh.0000125439.28861.ed.
36. **Zuern CS, Eick C, Rizas KD, Bauer S, Langer H, Gawaz M, Bauer A.** Impaired cardiac baroreflex sensitivity predicts response to renal sympathetic denervation in patients with resistant hypertension. *J Am Coll Cardiol* 62: 2124–2130, 2013. doi:10.1016/j.jacc.2013.07.046.

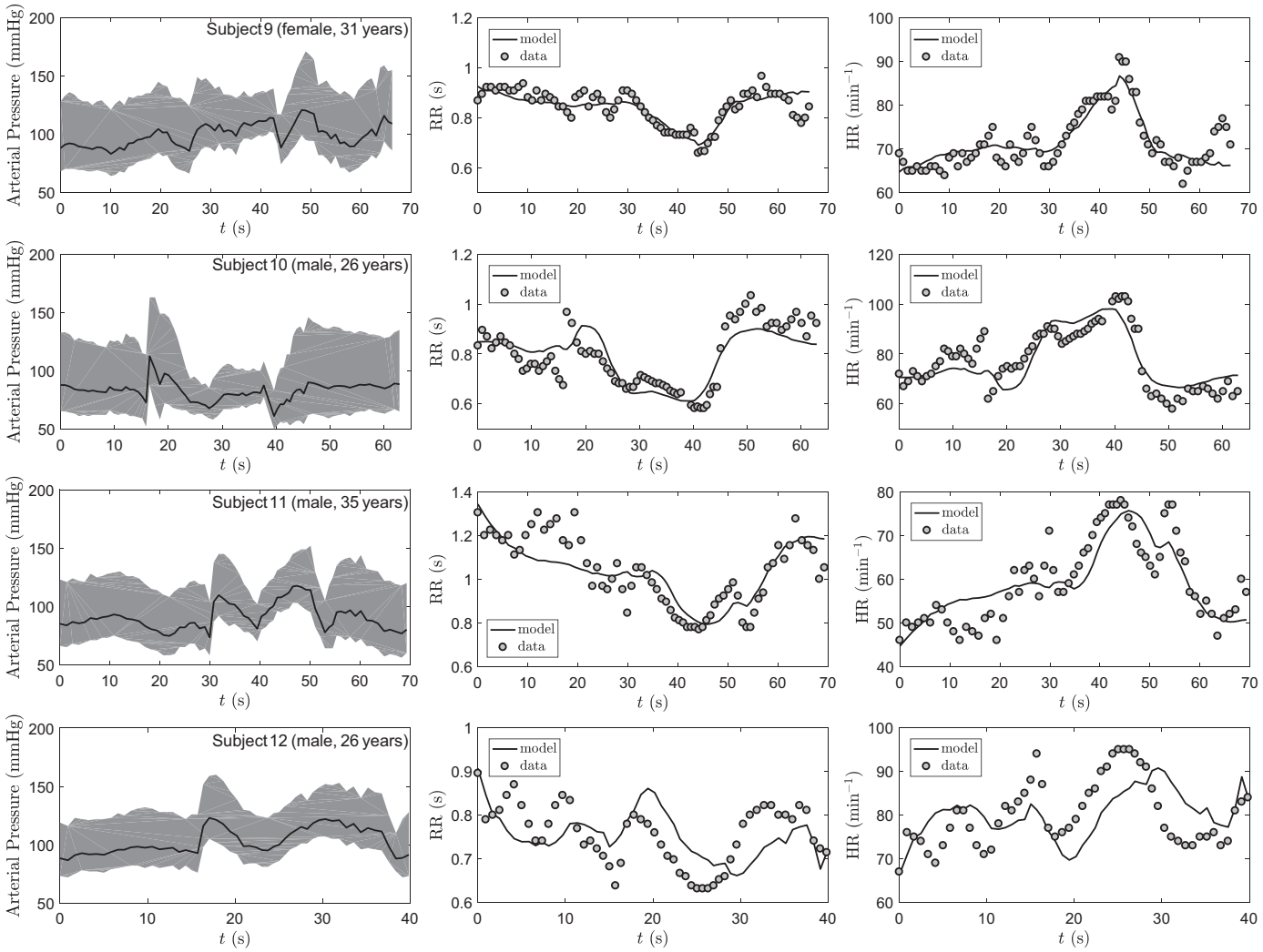

Fig. A3. Arterial pressures, R-R intervals, heart rate responses to Valsalva, and linear filter model fits for *subjects 9–12*. Panels at *left* illustrate measured arterial pressure, panels in *middle* illustrate measured R-R interval (RR) and fits of *Eq. 2*, and panels at *right* show the measured and model-fit heart rate (HR).

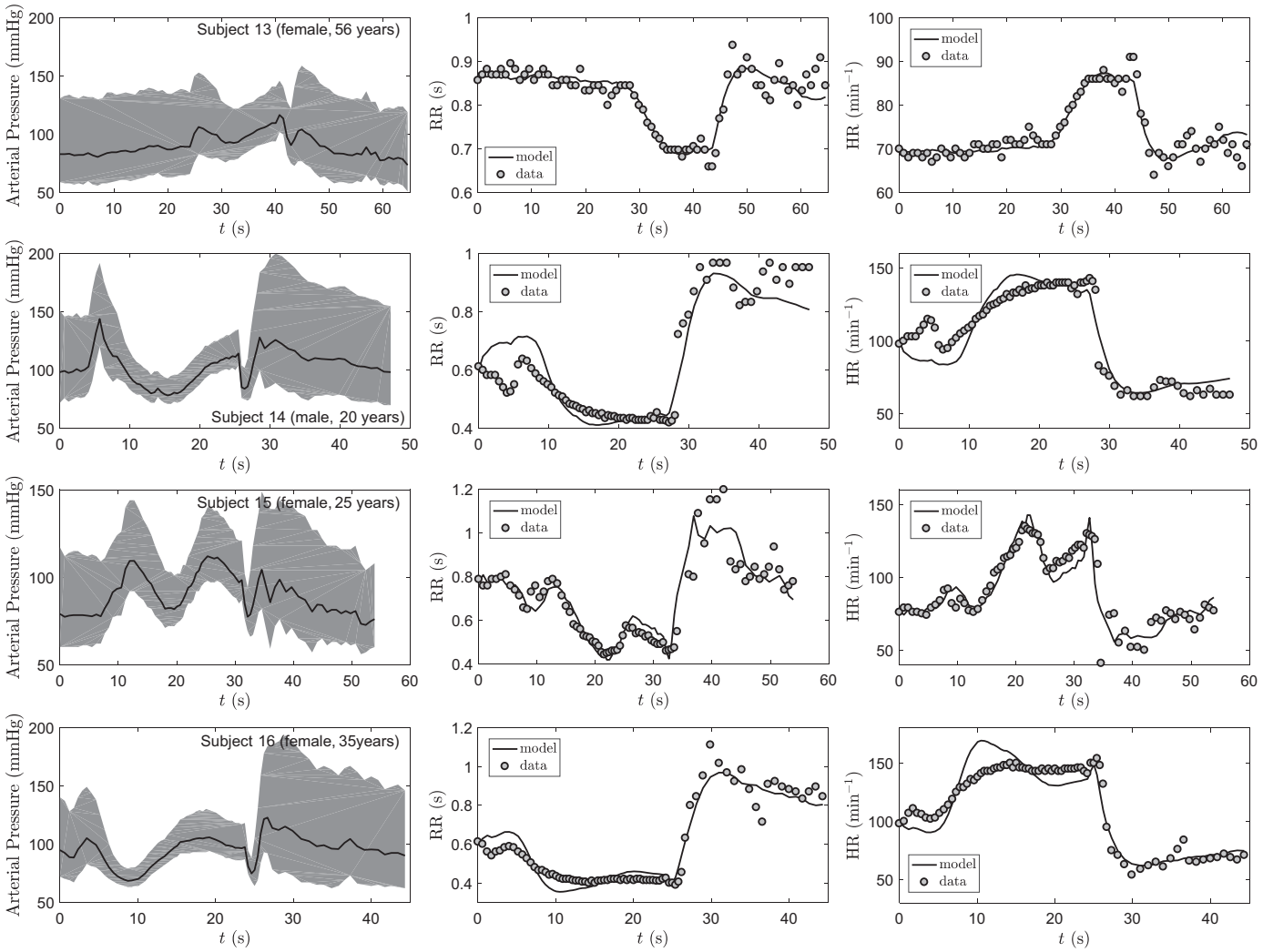

Fig. A4. Arterial pressures, R-R intervals, heart rate responses to Valsalva, and linear filter model fits for *subjects 13–16*. Panels at *left* illustrate measured arterial pressure, panels in *middle* illustrate measured R-R interval (RR) and fits of *Eq. 2*, and panels at *right* show the measured and model-fit heart rate (HR).

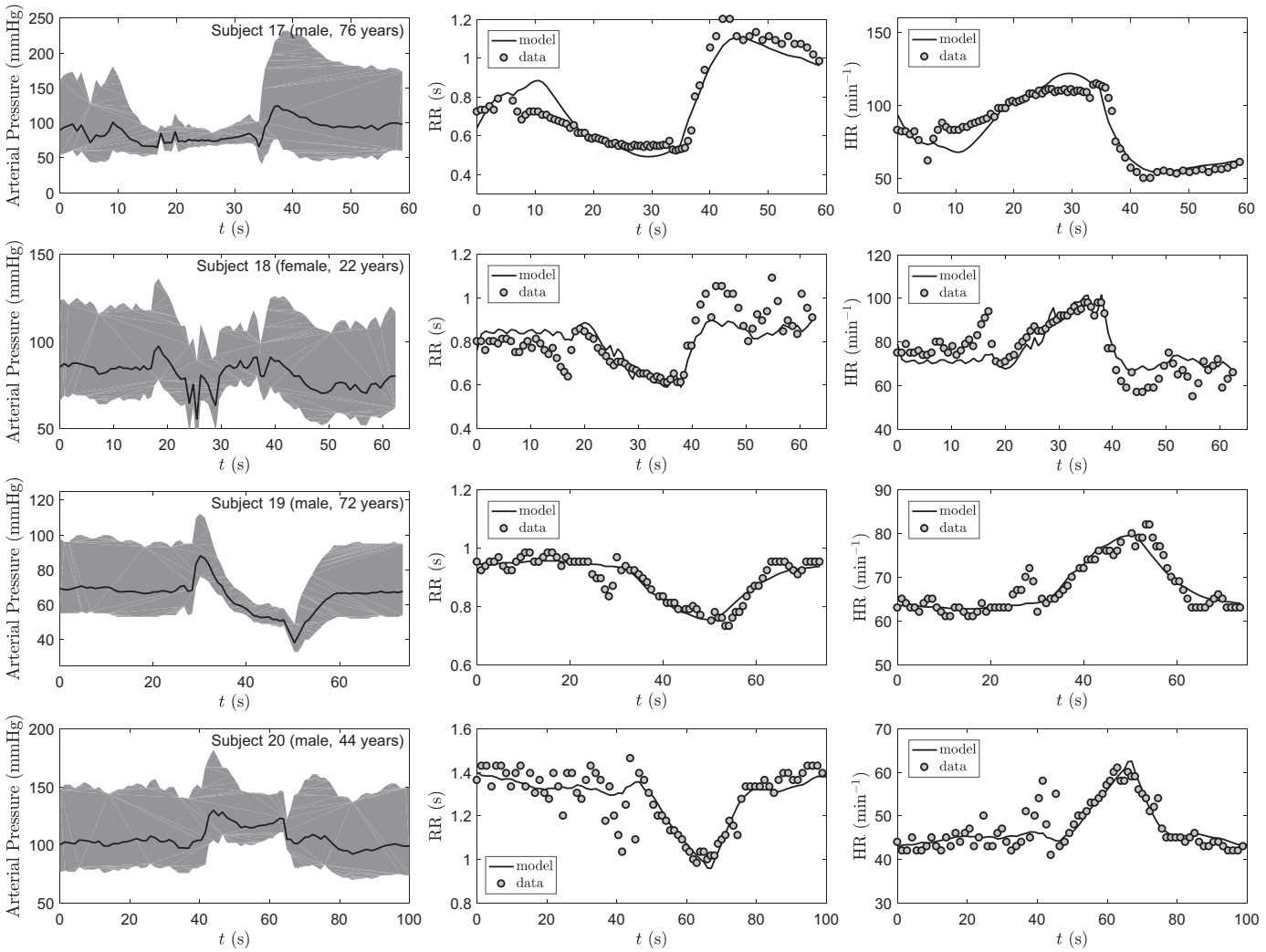

Fig. A5. Arterial pressures, R-R intervals, heart rate responses to Valsalva, and linear filter model fits for *subjects 17–20*. Panels at *left* illustrate measured arterial pressure; panels in *middle* illustrate measured R-R interval (RR) and fits of *Eq. 2*, and panels at *right* show the measured and model-fit heart rate (HR).

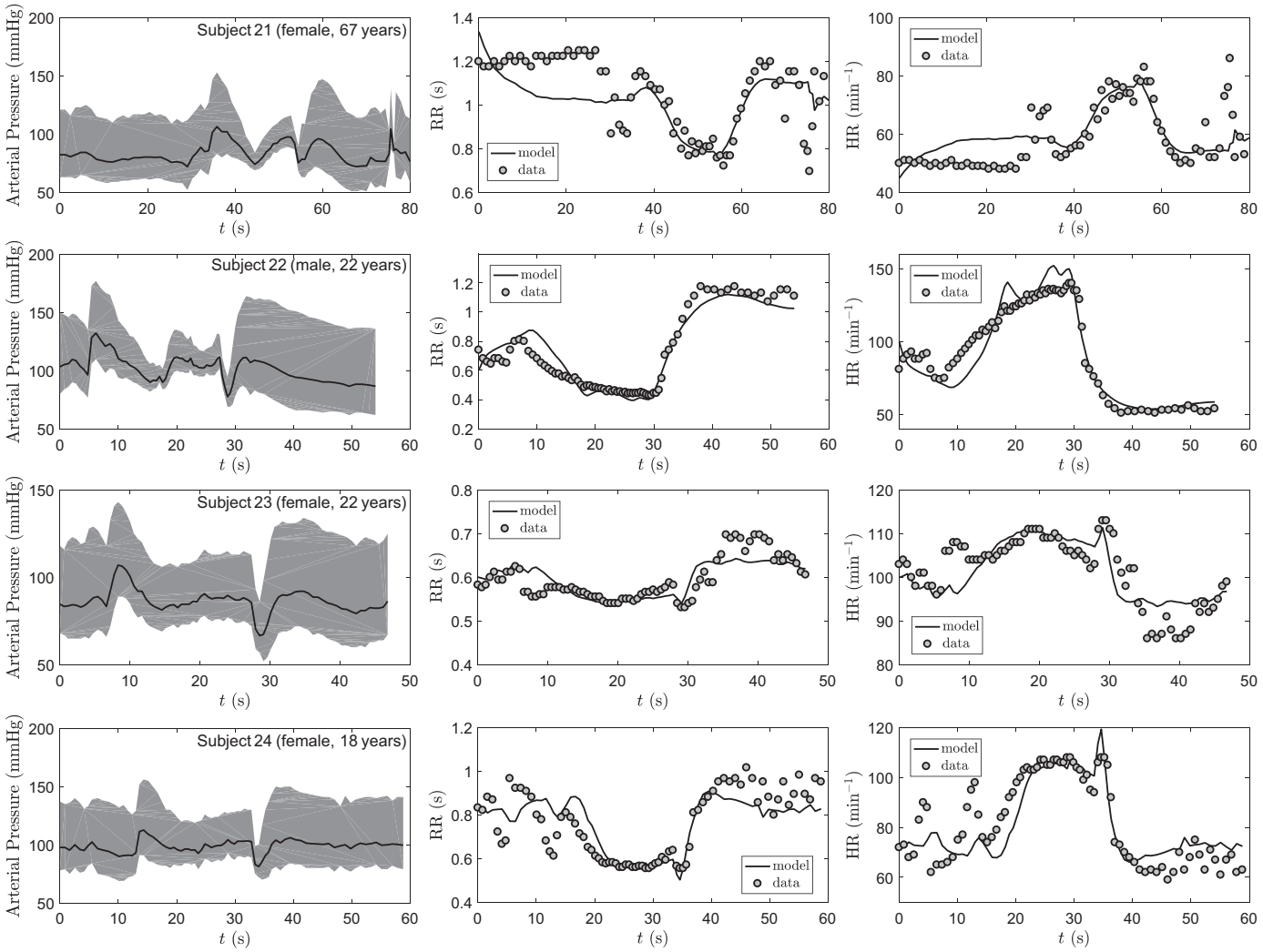

Fig. A6. Arterial pressures, R-R intervals, heart rate responses to Valsalva, and linear filter model fits for *subjects 21–24*. Panels at *left* illustrate measured arterial pressure, panels in *middle* illustrate measured R-R interval (RR) and fits of *Eq. 2*, and panels at *right* show the measured and model-fit heart rate (HR).

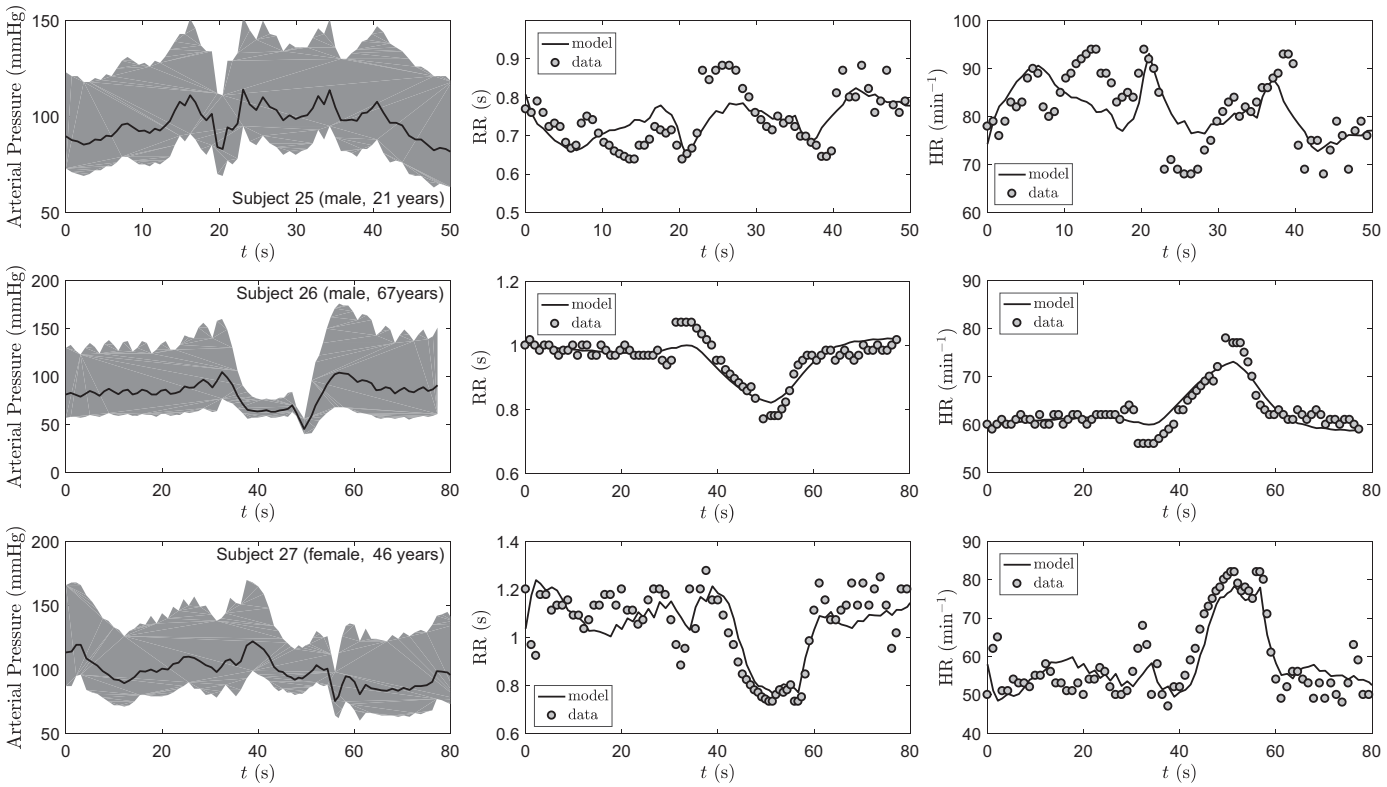

Fig. A7. Arterial pressures, R-R intervals, heart rate responses to Valsalva, and linear filter model fits for *subjects 25–27*. Panels at *left* illustrate measured arterial pressure, panels in *middle* illustrate measured R-R interval (RR) and fits of *Eq. 2*, and panels at *right* show the measured and model-fit heart rate (HR).

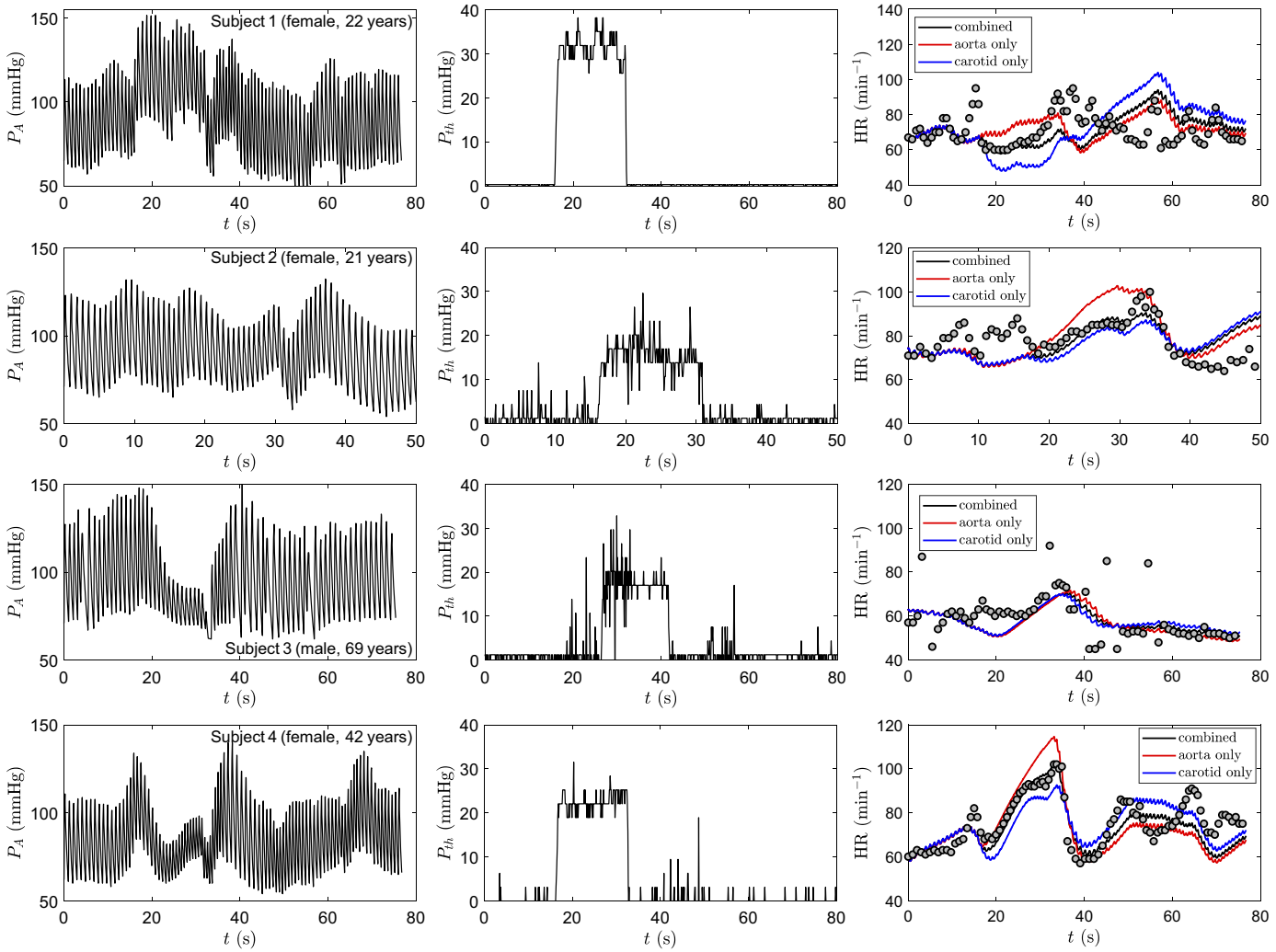

Fig. A8. Arterial and thoracic pressures, heart rate responses to Valsalva, and physiologically based model fits for *subjects 1–4*. Panels at *left* illustrate measured arterial pressure (P_A), panels in *middle* illustrate measured thoracic pressure (P_{th}), and panels at *right* show the measured and model-fit heart rate (HR).

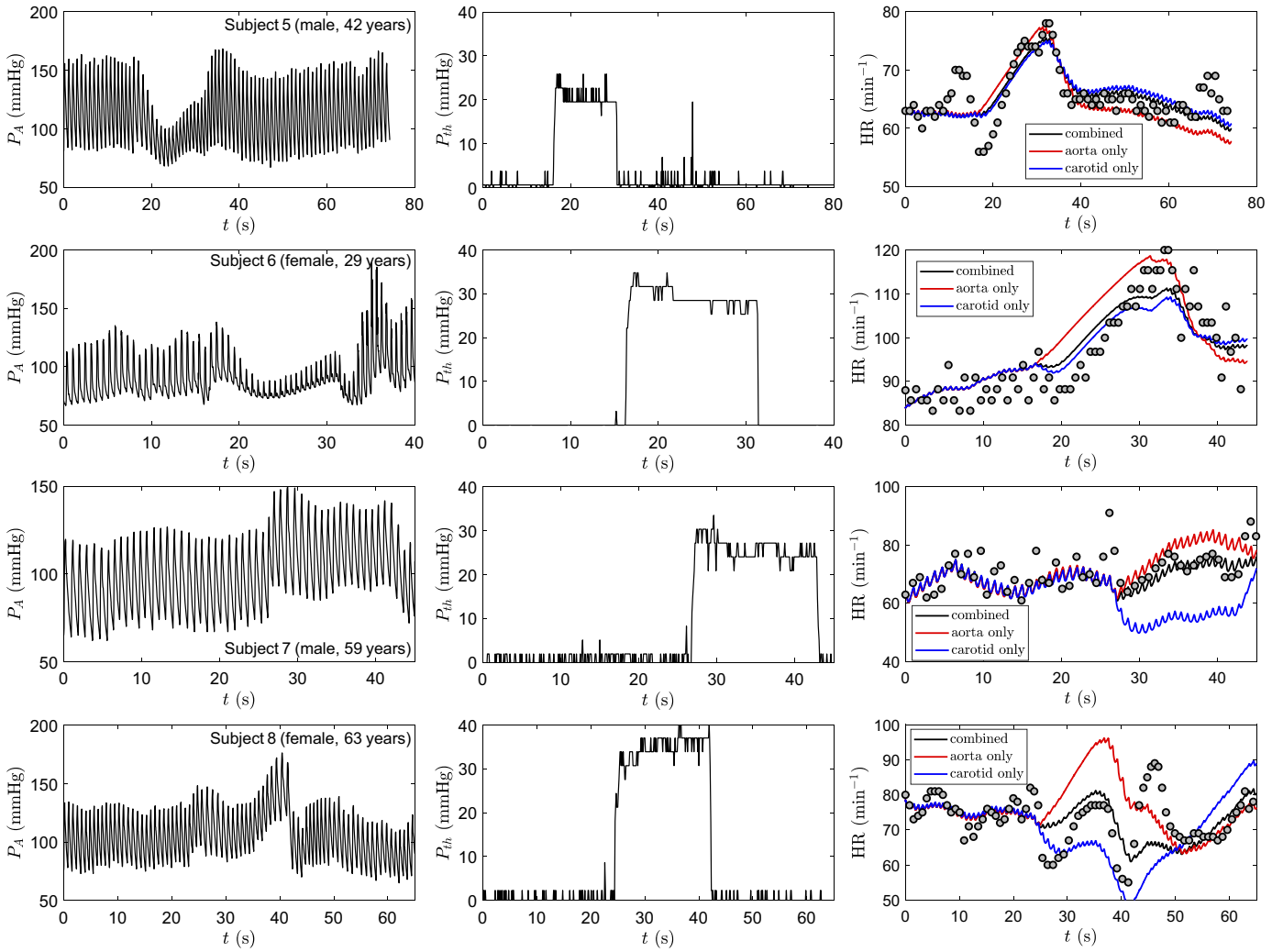

Fig. A9. Arterial and thoracic pressures, heart rate responses to Valsalva, and physiologically based model fits for *subjects 5–8*. Panels at *left* illustrate measured arterial pressure (P_A), panels in *middle* illustrate measured thoracic pressure (P_{th}), and panels at *right* show the measured and model-fit heart rate (HR).

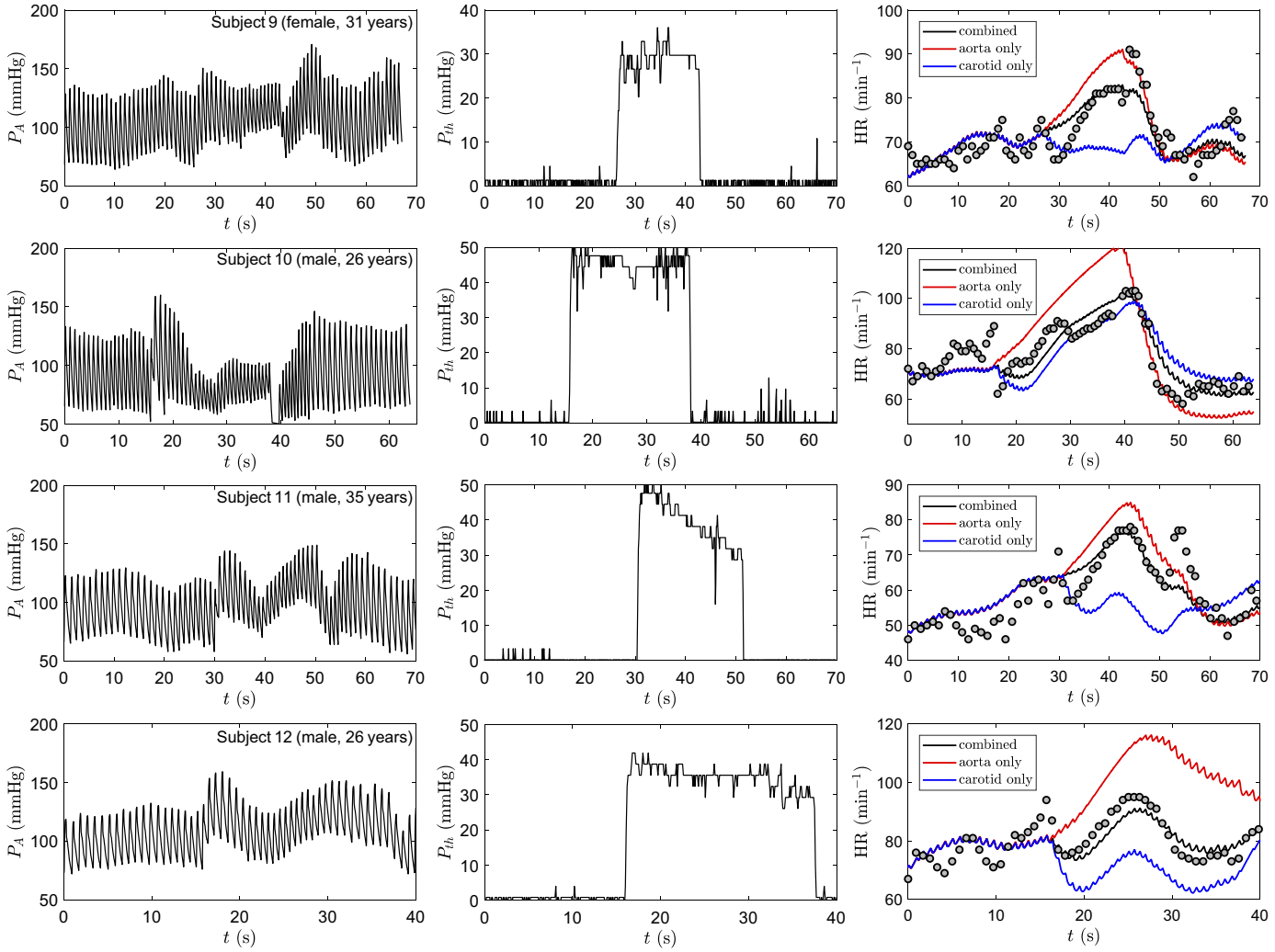

Fig. A10. Arterial and thoracic pressures, heart rate responses to Valsalva, and physiologically based model fits for *subjects 9–12*. Panels at *left* illustrate measured arterial pressure (P_A), panels in *middle* illustrate measured thoracic pressure (P_{th}), and panels at *right* show the measured and model-fit heart rate (HR).

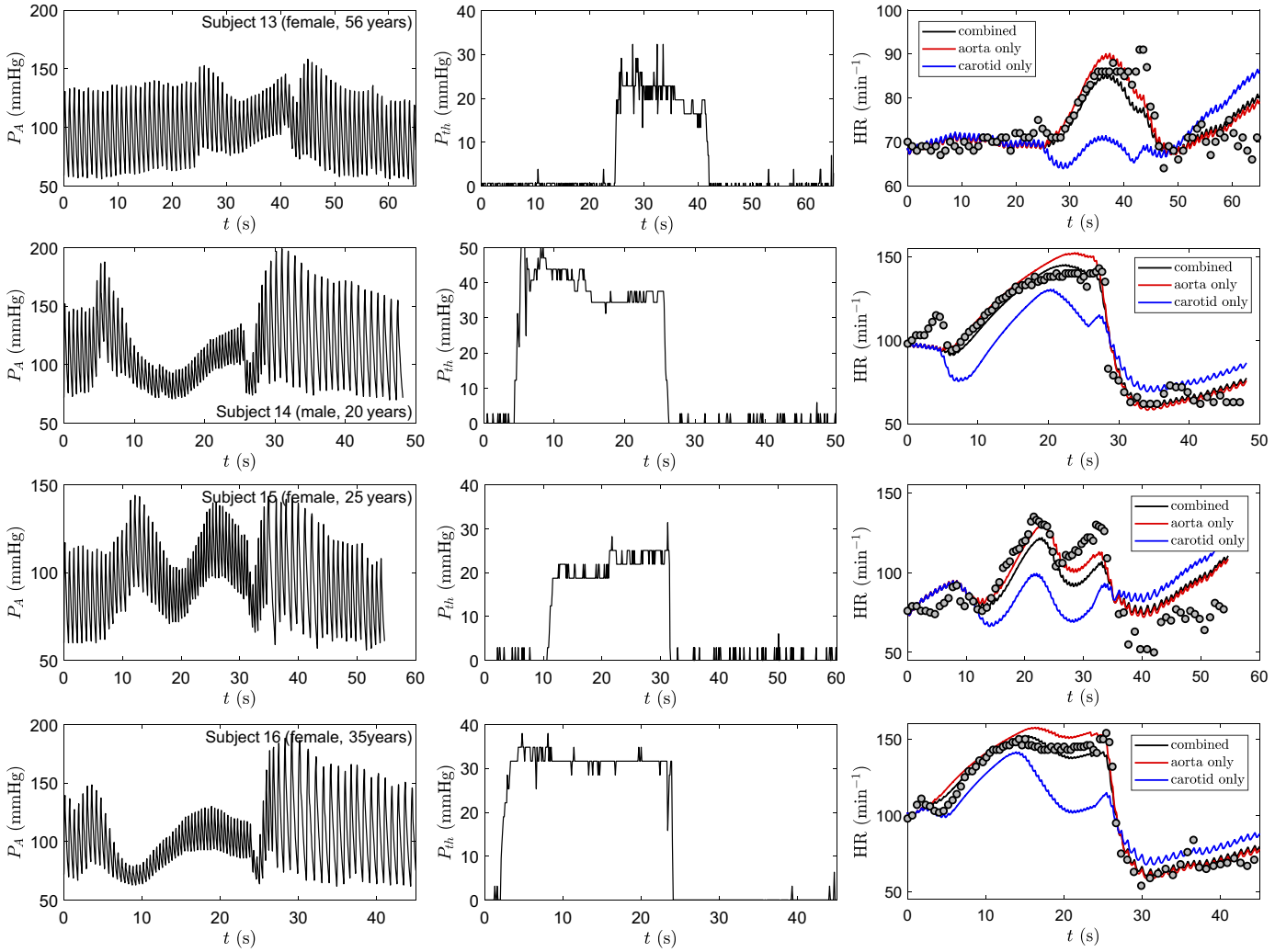

Fig. A11. Arterial and thoracic pressures, heart rate responses to Valsalva, and physiologically based model fits for *subjects 13–16*. Panels at *left* illustrate measured arterial pressure (P_A), panels in *middle* illustrate measured thoracic pressure (P_{th}), and panels at *right* show the measured and model-fit heart rate (HR).

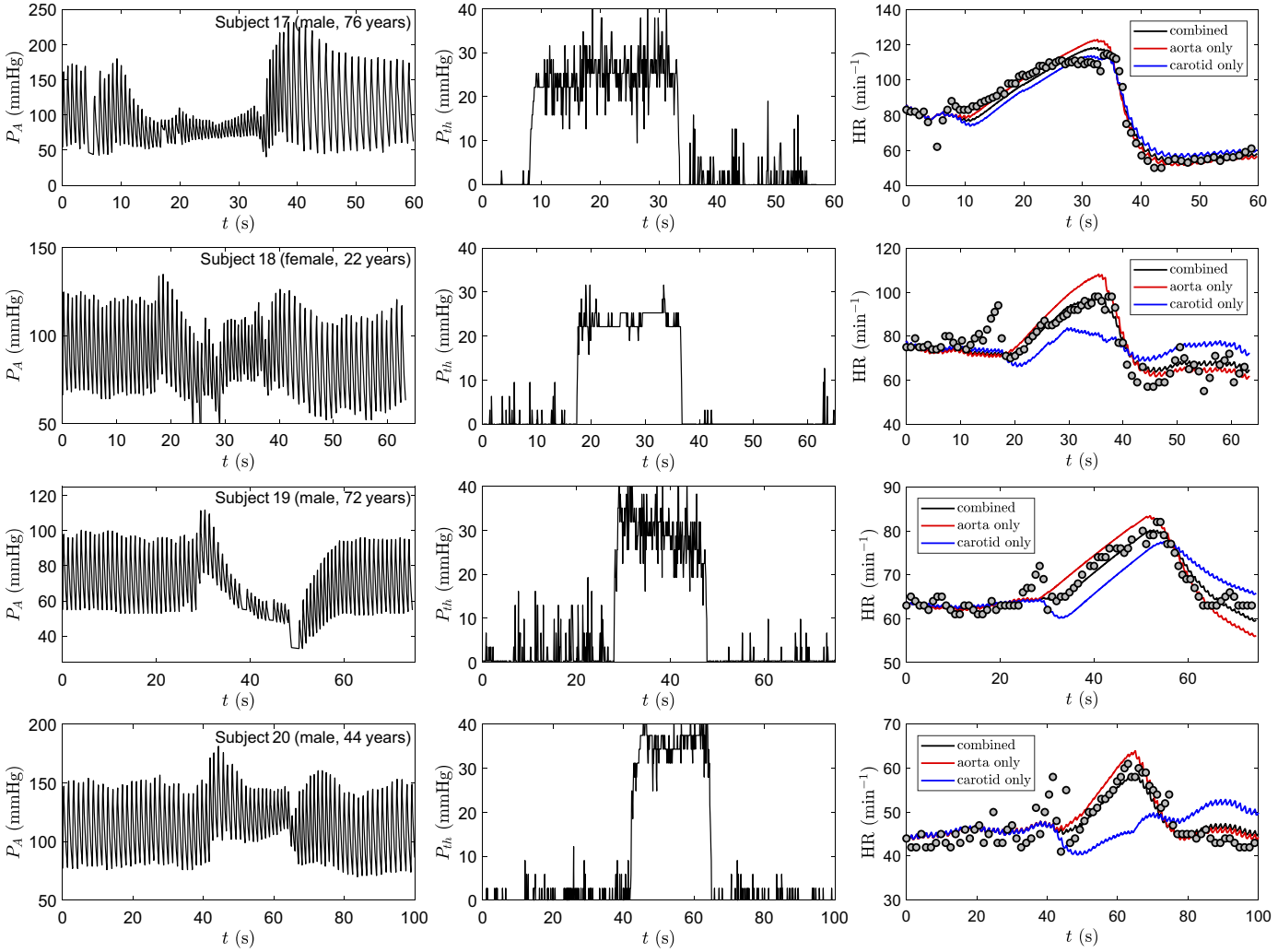

Fig. A12. Arterial and thoracic pressures, heart rate responses to Valsalva, and physiologically based model fits for *subjects 17–20*. Panels at *left* illustrate measured arterial pressure (P_A), panels in *middle* illustrate measured thoracic pressure (P_{th}), and panels at *right* show the measured and model-fit heart rate (HR).

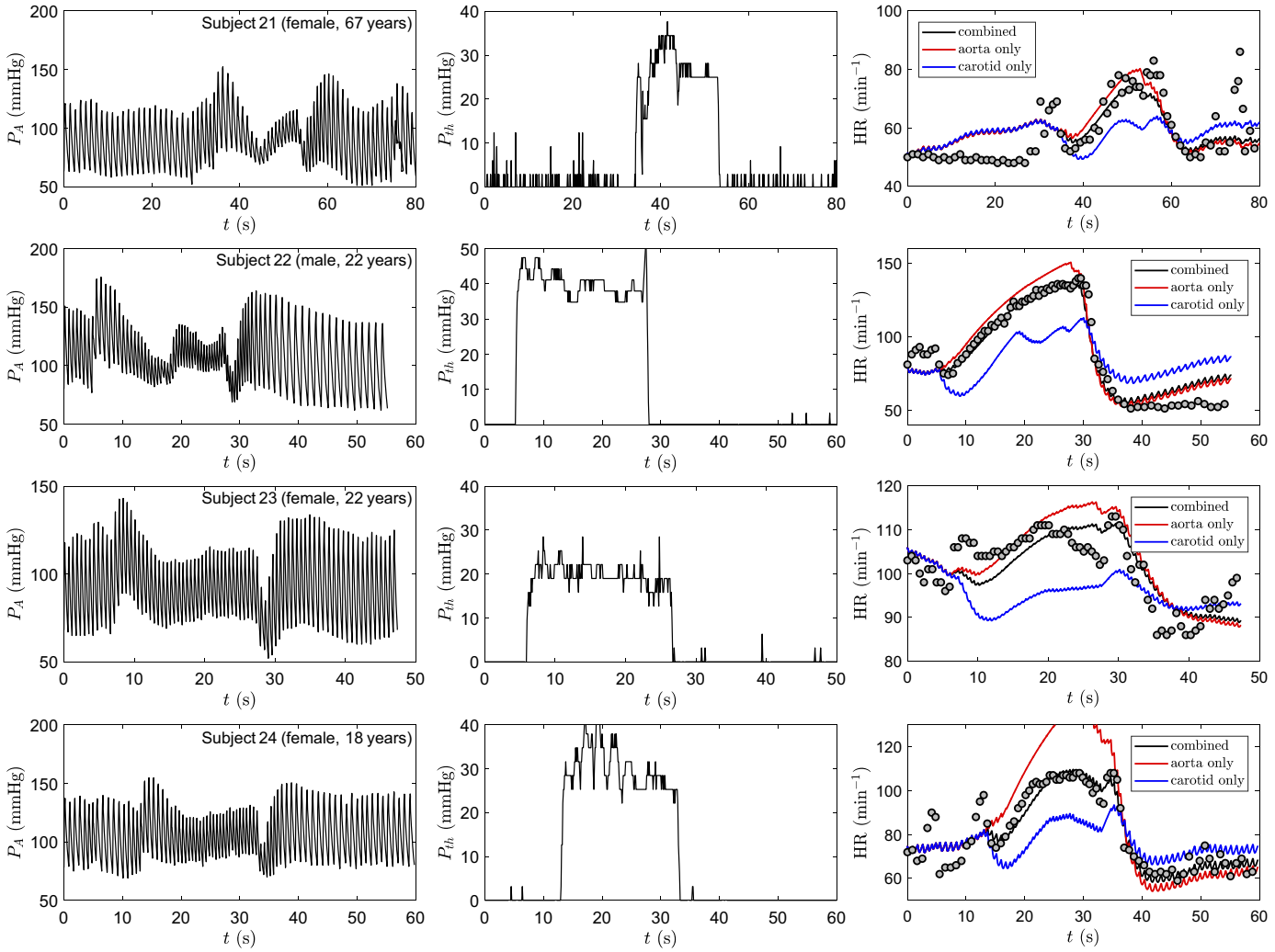

Fig. A13. Arterial and thoracic pressures, heart rate responses to Valsalva, and physiologically based model fits for *subjects 21–24*. Panels at *left* illustrate measured arterial pressure (P_A), panels in *middle* illustrate measured thoracic pressure (P_{th}), and panels at *right* show the measured and model-fit heart rate (HR).

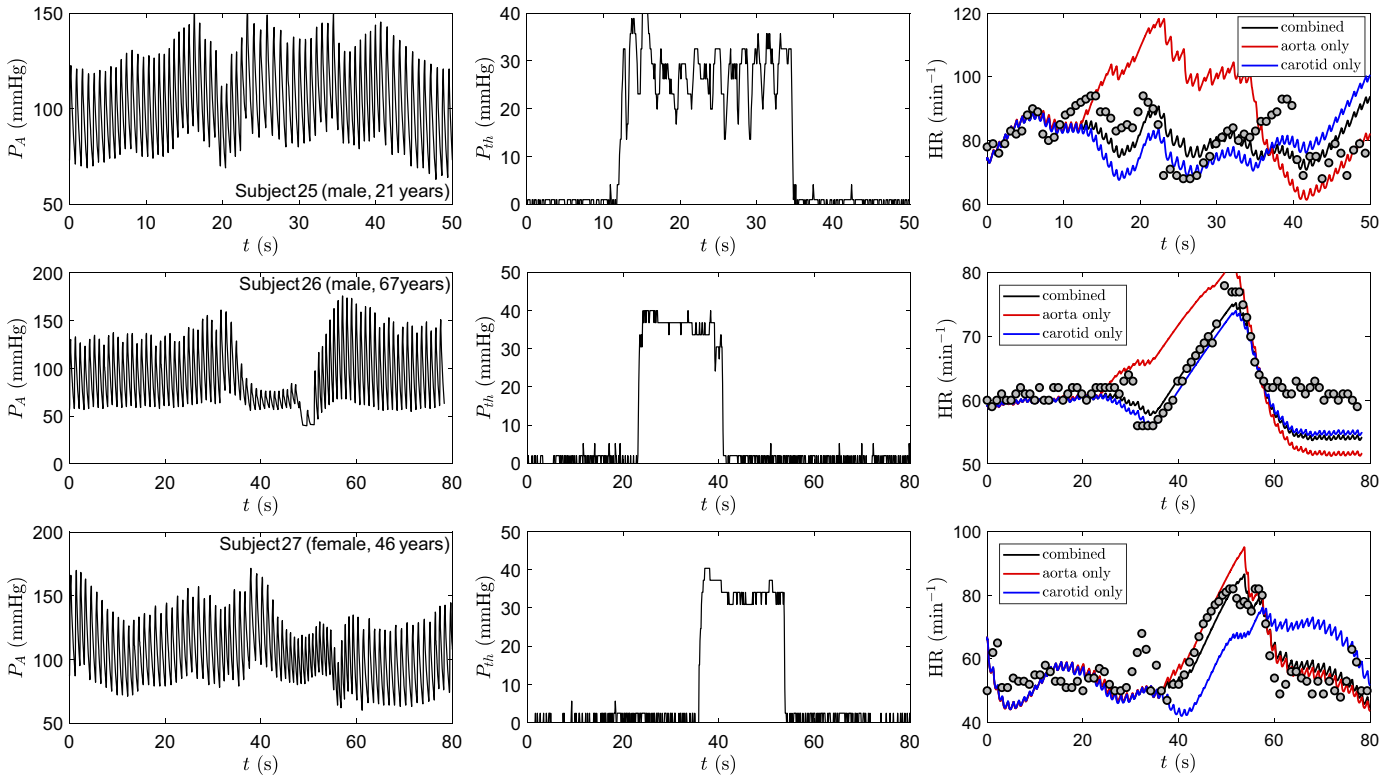

Fig. A14. Arterial and thoracic pressures, heart rate responses to Valsalva, and physiologically based model fits for *subjects 25–27*. Panels at *left* illustrate measured arterial pressure (P_A), panels in *middle* illustrate measured thoracic pressure (P_{th}), and panels at *right* show the measured and model-fit heart rate (HR).